Open access • Journal Article • DOI:10.1126/SCIROBOTICS.AAN4268

Self-healing soft pneumatic robots — Source link

Seppe Terryn, Joost Brancart, Dirk Lefeber, Guy Van Assche ...+1 more authors

Institutions: Vrije Universiteit Brussel

Published on: 16 Aug 2017

Topics: Soft robotics and Artificial muscle

Self-healing soft pneumatic robots

Terryn, Seppe; Brancart, Joost; Lefeber, Dirk; Van Assche, Guy; Vanderborght, Bram

Published in:
Science Robotics

DOI:
10.1126/scirobotics.aan4268

Publication date:
2017

Document Version:
Submitted manuscript

Self-healing soft pneumatic robots

Seppe Terryn[1,2], Joost Brancart[2], Dirk Lefeber[1], Guy Van Assche[2] and Bram Vanderborght[1]*.

Inspired by the compliance found in many organisms, soft robots are made almost entirely out of flexible, soft material, making them suitable for applications in uncertain, dynamic task-environments, including safe human-robot interactions. Their intrinsic compliance absorbs shocks and protects them against mechanical impacts. However, the soft materials used for their construction are highly susceptible to damage, like cuts and perforations caused by sharp objects present in the uncontrolled and unpredictable environments they operate in. In this research we propose to construct soft robotics entirely out of self-healing elastomers. Based on healing capacities found in nature, these polymers are given the ability to heal microscopic and macroscopic damage. Diels-Alder polymers, being thermoreversible covalent networks, were used to develop three applications of self-healing soft pneumatic actuators; a soft gripper, a soft hand, and artificial muscles. Soft pneumatic actuators commonly experience perforations and leaks due to excessive pressures or wear during operation. All three prototypes were designed, using finite element modelling, and mechanically characterized. The manufacturing method of the actuators exploits the self-healing behaviour of the materials, which can be recycled. Realistic macroscopic damage could be healed entirely using a mild heat treatment. At the location of the scar, no weak spots were created and the full performance of the actuators was nearly completely recovered after healing.

Introduction

With upcoming, new synthetic materials and the general trend of reducing weight and size in next generation robots, one subdomain, Soft Robotics (*1–4*) takes robotic compliance to the extreme. These soft robots consist almost entirely out of very soft, flexible, deformable materials (*5*), often elastomeric polymers such as Ecoflex®, which has a modulus of 10^5-10^6 Pa. Using these soft materials, an inherent compliance is created, which is comparable to the biological compliance of natural organisms (moduli 10^4-10^9 Pa) (*2*, *3*). This compliance match is key to safely interact in uncertain and dynamic task-environments including humans. Besides, soft robots can be used to move across rough terrain (*6*, *7*) or enter spaces through tiny cross sections (*8*). In contact with another object soft actuators can adapt their shape, making them good candidates for grippers (*9–13*) that have to handle soft objects, such as fruits or vegetables.

Because of their intrinsic softness, soft robots are resilient to mechanical impacts (*6*, *14*). However, softness comes at a price: the actuators are susceptible to cuts, shears, and punctures due to sharp objects, and as a vast part of soft robotics is pneumatic-actuated, also overpressuring is a common cause of damage. In this research we propose to solve this weakness by constructing soft robotics from synthetic self-healing (SH) soft materials (*15*), that permit healing microscopic and macroscopic damage. SH-materials are a relative recent technology, the term first emerging in 2001 (*16*, *17*). Since then a wide variety of SH-materials has been developed, relying on different physical and chemical principles (*18–21*). Some (commercial) applications have appeared in recent years, including SH-coatings (*22*) for cars and mobile phone covers that allow healing scratches. SH-asphalt and SH-concrete are on the verge of a commercial breakthrough (*23*). Puncture SH-polymers, already used in SH-targets, are being promising for aerospace applications (*24*) and artificial stretchable SH-films are been developed with high potential for artificial skin applications (*25*, *26*). However, so far this new material technology has barely made its entrance in the robotics, in which self-healing is only known on the software level (*27*).

Starting from preliminary studies (*15*), we prove that self-healing polymer networks that are cross-linked through a thermoreversible Diels-Alder reaction (*28*), can be used to develop soft pneumatic actuators that permit the healing of realistic, macroscopic damage caused by sharp objects or overloading. The Diels-Alder (DA) polymers (*29*) used are in essence non-autonomous SH-materials, as a trigger is needed to activate the reversibility of the bonds formation process. Macroscopic damage can be repaired in a couple of hours using mild heating as a trigger (> 70 °C). The need for a trigger, such as heat, complicates the healing procedure to some extent. However, it does provide an improved control over the process and a potentially infinite healing capacity. Of course, these non-autonomous SH-polymers can be turned into an autonomous SH-mechanism by combining them with a system that provides the trigger, in this case a heating device. Robots are ideal demonstrators for the integration of such a SH-mechanism, since they contain the power sources and control options required for the trigger system. Other SH-polymer approaches, like photo-induced SH-polymers (*30*) and supramolecular SH-polymers (*31*), certainly have potential for soft robotics too, but these will not be further elaborated here.

In this study, we introduce the SH-ability in three applications of soft pneumatic robots. A SH-soft hand (Fig. 1 A, D) was developed for applications where safe human-robot interactions are demanded, e.g. in social robots (*32*), household robots, and hand rehabilitation devices (*33*). Being active in non-preprogramed, dynamic environments, they are likely to encounter sharp objects such as metal edges, shattered glass, sharp plastics, or just the edge of a piece of paper. The fingers of the prototype (Fig. 1 A, D), which are based on existing bending actuator designs (*34*, *35*), are made entirely of flexible SH-polymers. Second, a SH-soft pneumatic gripper (Fig. 1B) was built using the same material. Because of the flexibility of the bending actuators, the gripper can handle a variety of soft objects without the need for extensive control and has potential to be used on sorting and packing lines of, e.g., the fruit and vegetable industry (*36*). Sharp objects like broken twigs can find their way into the lines and damage the gripper while sorting.

1) Robotics and Multibody Mechanics (R&MM), Vrije Universiteit Brussel (VUB) and Flanders Make, Pleinlaan 2, B-1050 Brussels, Belgium. http://mech.vub.ac.be/robotics.

*e-mail: bram.vanderborght@vub.ac.be

2) Physical Chemistry and Polymer Science (FYSC), Vrije Universiteit Brussel (VUB), Pleinlaan 2, B-1050 Brussels, Belgium. http://www.vub.ac.be/MACH/FYSC/.

The third application, are contractive pneumatic artificial muscles (*37*), often used in antagonistic setups to integrate compliance in robotic systems (*38*). They can produce high levels of forces at low to moderate speeds, excluding the need of (heavy) gearboxes. However, to produce high forces, high overpressures are required, which leads to increased wear and the formation of punctures and leaks, limiting the life cycle of the muscles. To deal with this, two self-healing pleated pneumatic artificial muscles (PPAM) (*37*) (Fig. 1C) were built. In all three applications, realistic damages could be healed entirely using a SH-procedure requiring mild heat (80 °C). No weak spots are created at the location of the scar and the actuator performances were almost entirely recovered after every healing cycle.

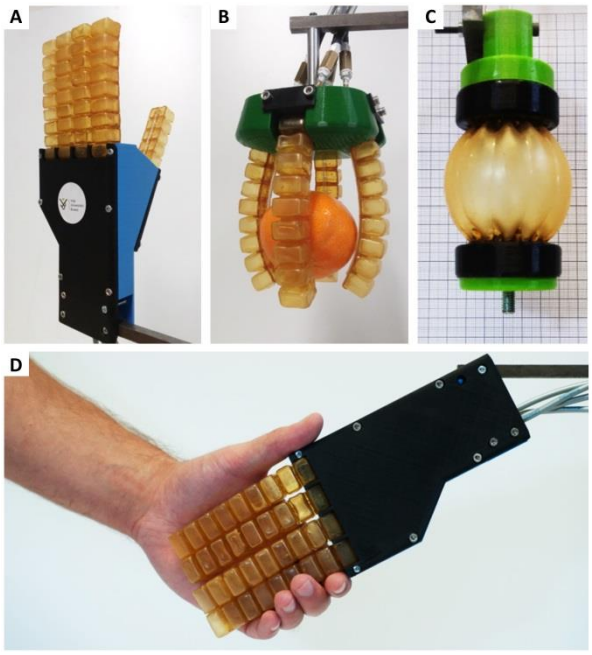

Fig. 1: Overview of the self-healing (SH) soft pneumatic actuators: (A and **D)** SH soft pneumatic hand. **(B)** SH soft pneumatic gripper. **(C)** SH pleated pneumatic artificial muscle.

In the search for new manufacturing techniques for soft robotics the reversible network formation that is the basis of the SH-ability of DA-polymers can be beneficial. Two separated surfaces of DA-components can be healed together, as illustrated by the "shaping-through-folding-and-self-healing" (*15*) approach used to construct all prototypes. This allows manufacturing DA-sheets into single SH-part with a more complex structure; the actuator prototypes. In addition we illustrate that DA-parts with completely different mechanical properties can be healed together as well to form single parts. Being manufactured from DA-polymers has an additional advantage; the SH-parts are remendable and therefore completely recyclable, which will be demonstrated in this paper. Soon soft robotics will leave the labs and make its entrance in industry and in our daily environment. We think it is important that this new technology is sustainable right from the start. In general, the use of self-healing/remendable polymers can have a contribution in the development of eco-friendly soft robotics. It can have beneficial impact on the life span of a wide variety of robotic components and reduce their over-dimensioning (*39*), lowering their ecological footprint. In addition, once a robot reaches the end of its usefulness, its SH-components can be completely recycled and reused.

The paper presents healing experiments on DA-polymer samples to illustrate and describe the SH-ability. The visco-elastic and mechanical properties of the synthesized DA-polymers are measured and their potential for their use for soft robotic applications is evaluated. For each SH-actuator application, prototypes were designed using finite element modelling and manufactured using a shaping method exploiting the self-healing capacity of the materials. The mechanical performance of the prototypes was measured and compared with soft robots in literature and their healing capacity was evaluated for realistic damage to the membranes of the actuators. The recovery of the properties of the SH-polymers and the performance of the soft actuators after multiple SH-cycles is validated.

Results

Self-healing based on reversible Diels-Alder bonds

The healing capacity of the soft actuators is based on the Diels-Alder (DA) reactions between a diene (furan) and a dienophile (maleimide) (*29*) (Fig. 2A), which form thermoreversible cross-links in the polymer network (Fig. 2B). The exothermal DA-reaction is an equilibrium reaction for which the equilibrium extent of the reaction is a mild function of temperature. The SH-procedure can be split into five stages illustrated in Fig. 3, along with microscopic images of DA-polymer samples at the different stages (Movie S1). *Damage:* first the polymer is damaged, e.g., by making a cut with a sharp object or a perforation by applying excessive overpressure. At the location of the damage, the DA-bonds are mechanically broken, because these are the weakest of the network. *Heating:* The healing action is activated by means of a heat stimulus (for our systems 80 °C suffices). By increasing the temperature, the equilibrium is shifted from a major fraction of formed DA-bonds towards the breaking of these bonds and the formation of furan and maleimide functional groups. As a result, the mobility of the polymer

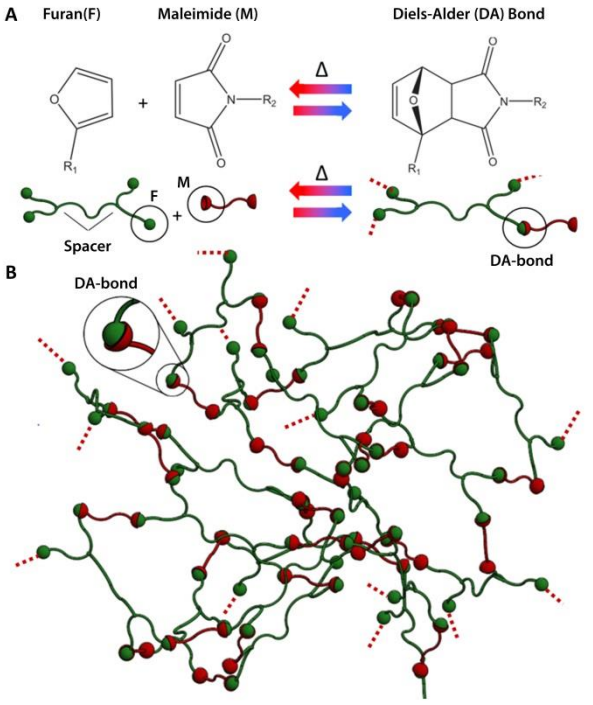

Fig. 2: The thermoreversible network formed by the DA-cross-links. (A) The equilibrium DA-reaction: at low temperatures, the network is formed due to high conversion to the DA-bonds. At high temperatures, these DA-bonds fall apart and the mobility of the polymer chains increases. **(B)** Thermo-reversible elastomeric network formed by cross-links of the reversible Diels-Alder bond.

chains in the network will be increased. *Isothermal stage:* Staying at these temperatures will further increase the mobility by breaking cross-links as the reaction progresses to the new equilibrium, up to a point where the polymer has enough mobility and enough time to seal the gap/cut (typically 20-40 min).

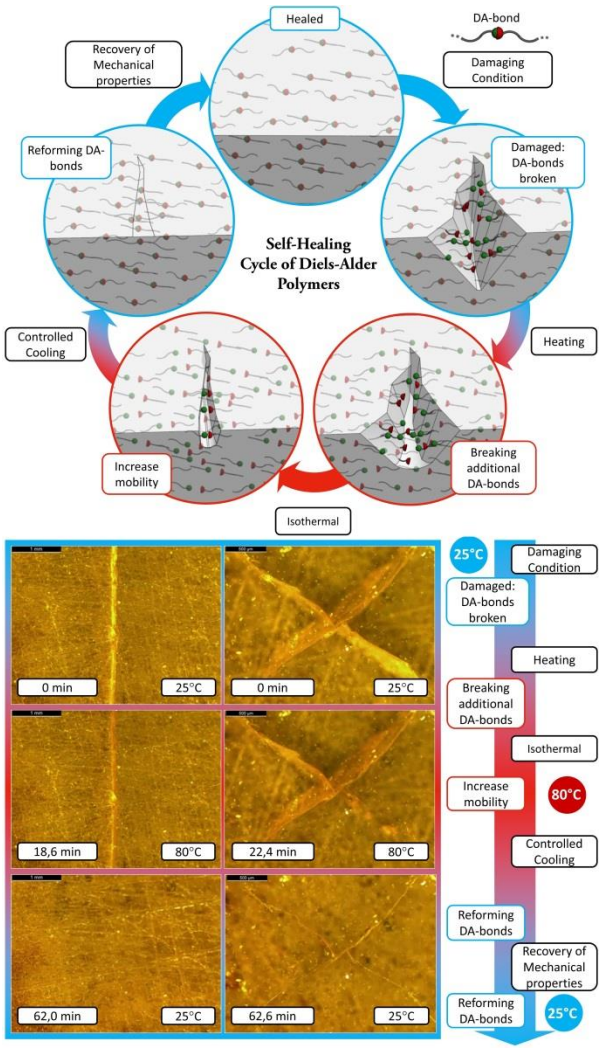

Fig. 3: Schematic of the SH-cycle of DA-polymers. The SH-procedure contains 5 steps: the damage, a heating step, an isothermal step, a controlled cooling and a recovery at room temperature. The pictures illustrate the self-healing of a damaged DA-polymer sample (DPBM-FGE-J4000) during the different stages (Movie S 1).

Controlled cooling: When the damage is sealed, the temperature can be decreased. Upon cooling, the shift of the equilibrium is reversed, resulting in the gradually re-forming of the cross-links in the network (Fig. 2B), which is the basis for restoring the properties of these DA-polymers. It is important to perform this with a low cooling gradient, since this enhances the recovery of the initial mechanical properties and reduces the total duration of the SH-procedure. *Recovery at ambient temperature:* At room temperature, the initial mechanical properties have to be fully recovered. Slow cooling followed by a sufficiently long waiting time at ambient temperature offers a good compromise between the decelerating kinetics and the increasing thermodynamic driving force for the formation of the bonds. Using a cooling rate of 2 $K.min^{-1}$, this last step takes around 22 hours according to simulations (Fig. S 3). The complete temperature profile of the healing can be found in Fig. S 4.

Thermal and mechanical properties of the DA-material

The mechanical properties at ambient temperature and during healing can be tuned during the synthesis (Fig. S 1) of the DA-polymer. For this work, the length of the Jeffamine spacer used for synthesizing the furan-functionalized building block (Fig. 2A) was varied (*15*, *29*, *40*). For shorter spacer lengths (J400, 400 $g.mol^{-1}$), a polymer network (Fig. 2B) is created with a higher crosslink density, resulting in a glassy material with a storage modulus of 1.6 GPa and a strain at fracture of only 1.6%. When the spacer length is longer (J2000, 2000 $g.mol^{-1}$ and J4000, 4000 $g.mol^{-1}$) are obtained. The J4000 results in the most flexible material of the series, with a storage modulus of 13 MPa and a strain at fracture of 360%. A summary of the thermal and mechanical properties of the three basic DA-polymers is presented in Table 1 (Experimental results can be found in Fig. S 5, Fig. S 6, Fig. S 7 and Fig. S 8). For the properties where a standard deviation is provided, 4 samples were measured. Many other variations can be made during the synthesis. By combining Jeffamines with different chain lengths, the entire range of mechanical properties between the most flexible J4000 and most brittle J400 can be synthesised. This allows tuning the DA-polymers for diverse robotic applications. In previous work, the brittle J400-based thermoset was used to construct a self-healing mechanical fuse (*39*) that can protect a robotic actuator. The flexible J4000 elastomer is used to construct the soft robots (Fig. 1) in this paper.

Table 1: Thermal and mechanical properties of DA-materials synthesized using different Jeffamine Jx spacers.

Properties		J4000	J2000	J400
Glass (g) and gel Transition Temperatures				
DMA: Tg	°C	-48.5 ± 0.4	-43.6 ± 2.4	74.7 ± 1.7
Rheology: Tgel	°C	98 ± 1	119 ± 1	
DMA Properties: 25°C, 1 Hz, 0.5 % (J4000), 0.5% (J2000), 0.1% (J400)				
Storage Modulus	MPa	12.9 ± 1.3	107.4 ± 26.0	1602.5 ± 431.5
Loss Modulus	MPa	1.79 ± 0.14	19.3 ± 2.9	79.6 ± 21.7
Tan(δ)		0.139 ± 0.004	0.183 ± 0.021	0.055 ± 0.026
Stress Stain Curve: 25°C, 65 %/min (J4000 and J2000) 0,1 %/min (J400)				
Fracture Strain	%	356 ± 19	353 ± 31	1.58 ± 0.07
Fracture Stress	MPa	1.88 ± 0,07	6.85 ± 0.29	20.9 ± 1.8
Young Modulus	MPa	5.0 ± 0.1	66.3 ± 5.5	1755 ± 78
Density	g/ml	1.05 ± 0.03	1.13 ± 0.02	1.19 ± 0.01

Design of the bending soft pneumatic actuator

To demonstrate the potential of DA-polymers in existing soft robots, we decided to build a Pneu-Net actuator (*41*). These are made up of a series of channels and chambers constructed in an elastomer, usually a hyper elastic material like Ecoflex® 0030 (Young's modulus of 67 kPa). When the chambers are pressurized, they inflate and motion is created. All kinds of motions are created using different Pneu-Net designs (*7*, *8*, *34*, *41*), but the one mostly used in soft gripper/hand applications (*36*), is the bending soft pneumatic actuator (BSPA) (*35*, *42*). In these applications the hyper flexible BSPA can easily get damaged by all kinds of sharp objects, making it an ideal demonstrators for the introduction of SH DA-elastomers in the soft pneumatic robotics. A BSPA prototype was designed and constructed almost entirely out of DA-polymer (Fig. 4 A, B and Fig. S 10).

The BSPA actuator is a cuboid in which a series of 9 inflatable air chambers (cells) is embedded. A flexible tube is integrated in the bottom layer that connects all of the 9 cells to the same pressure source, such that all can be pressurized simultaneously. The entire actuator is constructed out of the

most flexible self-healing DA-polymer, the DPBM-FGE-J4000, except from the flexible tube that is made out of Tygon R3603. The bottom layer, connecting all chambers and containing the flexible tube, is thicker, allowing very little planar strain. Consequently, pressurization of the air chambers produces inflation on the top and side surfaces, while the strain at the bottom surface remains essentially zero. As the expanding outer walls of the cells start making contact, a bending motion is produced (Fig. 4 A, B), where the distance between the two ends of the actuator decreases as the curvature increases. The same principle has led to the development of actuators that respond to pressurization with a wide range of motions: bending, extension, contraction, twisting and others.

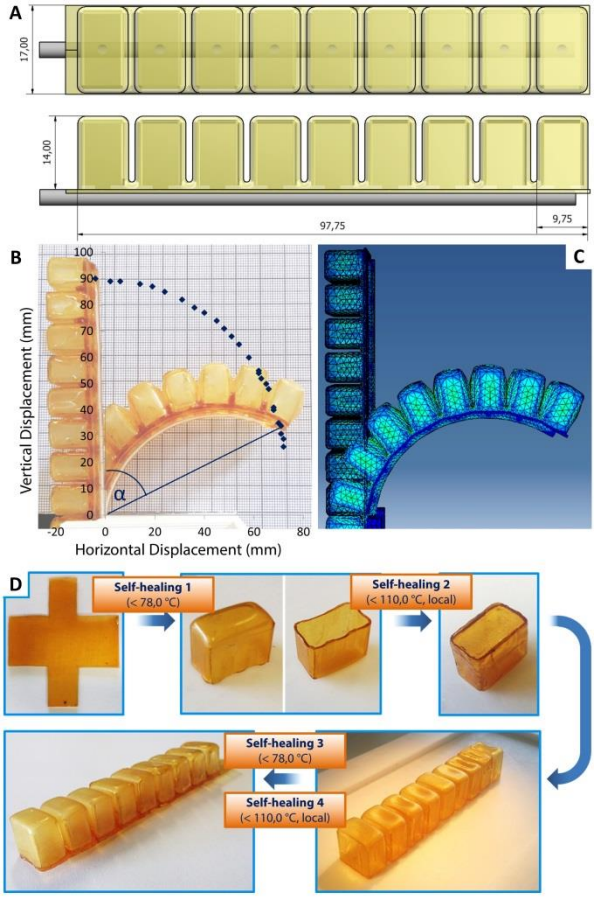

Fig. 4: Design and manufacturing of the SH-BSPA: **(A)** Dimensions (in mm) (detailed datasheets in Fig. S 10). **(C)** Illustration of the bending motion caused by an overpressure in the air chambers. **(C)** Abaqus simulation for large deformations at 30 kPa (Fig. S 9 and Movie S 2). **(D)** Building the BSPA: through folding and self-healing procedures (< 78 °C globally and < 110 °C locally) connections are made between the different parts and the actuator is made airtight (Fig. S 12).

The design was fine-tuned by simulating large deformations, using a static elastic model in Abaqus (Fig. 4C, Fig. S 9 and Movie S 2). The elastic deformation response is modelled using the Young's modulus of the DA-material (J4000-based, 5.0 MPa) and the flexible tube (1.1 MPa). Because of the relative small strains (max. 30%) and limited pressurization times (typically a few minutes), visco-elastic response effects of the polymers did not have to be accounted for. Gravity was accounted for (densities: J4000, 1.05 g/ml and tube, 1.00 g/ml). Numerical simulations indicated that slightly decreasing the wall thickness of the cells while maintaining a sufficiently rigid bottom sheet results in an increase in curvature of the BSPA. To evaluate this in practice, BSPAs were constructed with a wall thickness of 0.75 mm (BSPA 1 and 2) and 0.60 mm (BSPA 3 and 4) (Fig. S 10).

Shaping soft robots using the self-healing ability

The SH-ability of DA-polymers can offer great benefits for the manufacturing of (self-healing) soft robots. We developed a shaping method to produce 3D polygon structures starting from 2D sheets of SH-polymers by combining folding and healing steps. The process, which we named "shaping-through-folding-and-self-healing" (*15*) was used to manufacture all the SH-prototypes (Fig. 1) and will be illustrated with the shaping process of the BSPA (Fig. 4E). In total four healing steps were needed to develop the prototype.

After synthesis of the building block, the DA-material is solvent-cast into sheets (Fig. S 1 and Fig. S 12). To construct the cells of the SPA, a plus sign was cut out of a J4000-based sheet. The plus-shaped geometry is folded into an open rectangular cuboid shape. The sides of the cuboid are sealed and made airtight by subjecting the cuboid to a heat treatment in an oven (78 °C for 2 hours, cooling at ± 0.5 K min^{-1}), using the SH-ability. A single cell is formed by closing the box using a slightly larger square of J4000-based sheet. The cell is made airtight by locally heating the joints up to 110 °C for seconds only (using a soldering tool). To complete the actuator, 9 cells are placed in series and are fixed to a bottom J4000-based sheet, containing the flexible tube, using a third SH-procedure (78 °C for 30 min, cooling at ± 0.5 K min^{-1}). An additional local heating was used to make sure the bottom sides were completely airtight.

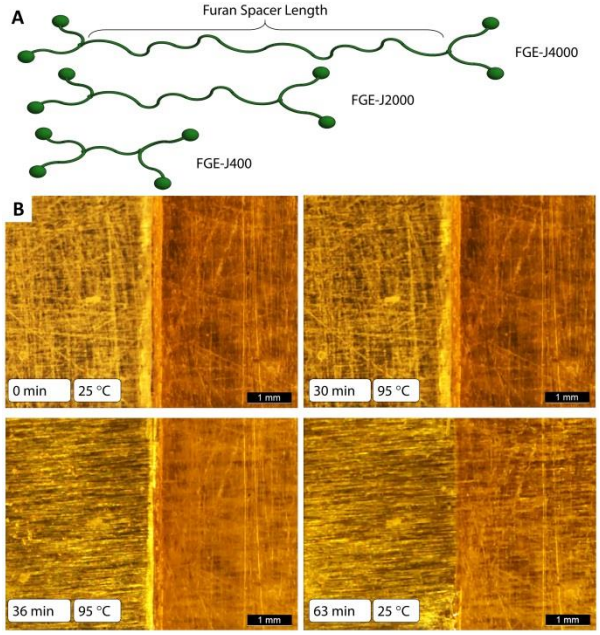

Fig. 5: DA-sheets with completely different mechanical properties can be seamlessly healed together. (A) Using different Jeffamines (D400, D2000, D4000) furan-functionalized building blocks (FGE-Jx) with different spacer length can by synthesized. **(B)** Because the J4000 and J2000 DA-polymers differ only in furan spacer length, the materials can be self-healed together using a SH-procedure with a maximum temperature of 95 °C (Movie S 3). The initial gap between the sheets was 0.3 mm.

As the thermo-reversibility of the different DA-polymers originates from the same reversible Diels Alder cross-links, polymers with completely different mechanical properties can be fused together to form a single part, using their SH-ability, while the connection becoming as strong as the materials themselves. Fig. 5B shows optical microscopy images of the edge of a J4000-based and a J2000-based sheet that are fused together in healing procedure (Movie S 3). The initial gap (0.3 mm) at the top of the two sheets was completely sealed. The surfaces of the two sides were also smoothened, since microscopic scratches were also healed. The fact that combining different DA-polymers is perfectly feasible, strongly increases the degree of freedom during the design phase of soft robotics since single parts can be created, consisting of materials with different properties.

Mechanical properties of the soft pneumatic actuator

Four bending soft pneumatic actuators prototypes were constructed and characterized using a dedicated test setup, containing a pressure control system (Fig. S 14 and Fig. S 15). The characteristics of the four BSPAs can be found in Fig. 6 A, B and C. The variation in behaviour between SPAs 1 and 2 versus SPAs 3 and 4 is due to the difference in sheet thickness of the cells, which are 0.75 mm and 0.60 mm, respectively (Fig. S 10). The deformations of the actuator were captured for various overpressures, using a digital camera (Fig. 4B). The four bending actuators follow nearly the same curvature trajectory (Fig. 6A), which is necessary for soft hand and soft gripper applications in which well-controlled movement is required.

The bending angle α, defined in Fig. 4B, is presented as a function of the overpressure in the air chambers in Fig. 6B. It is clear that BSPA 1 and 2 have very similar characteristics, which is also the case for BSPA 3 and 4. This indicates that shaping-through-folding-and-self-healing allows producing bending actuators in a reliable manner. Bending angles up to 70° could be achieved for overpressures around 25.0 kPa and decreasing the wall thickness leads to more flexible, softer actuators. The force exerted by the tip of the bending actuators on a surface was measured for different overpressures (Fig. 6C). Forces of about 0.25 and 0.32 N

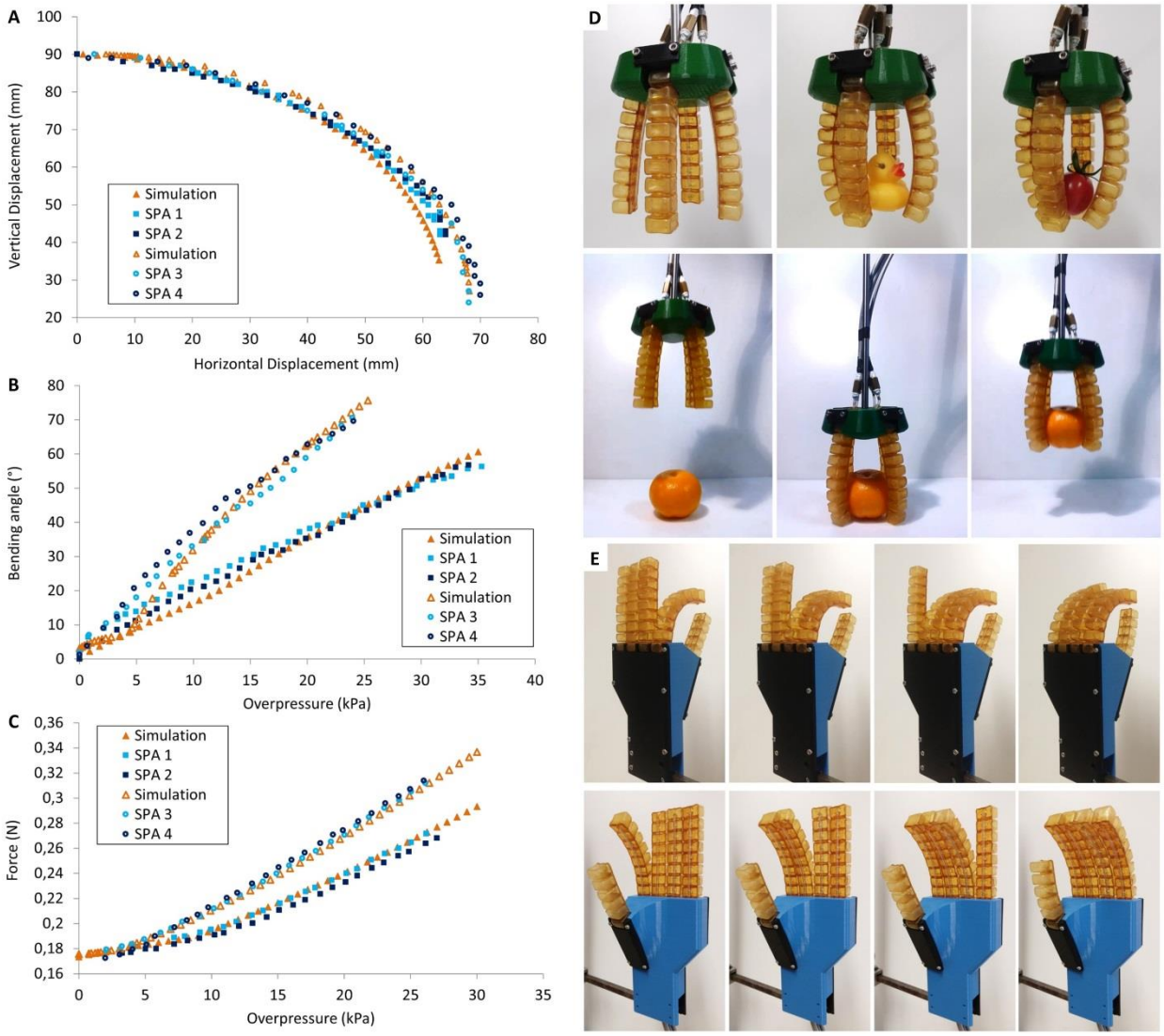

Fig. 6: Mechanical characteristics of the four BSPAs and their functionality in a soft gripper and a soft hand. The experimental measurements are compared to the numerical simulations using static elastic models in Abaqus: **(A)** Vertical and horizontal displacement of the actuator tip for different overpressures. **(B)** Bending angle as a function of the overpressure. **(C)** Force exerted by the tip of the BSPA. **(D)** Operating the four BSPAs in a soft pneumatic gripper. The overpressure in the actuators can be regulated individually. This allows exerting simultaneously the same force on the object with each actuator to create smooth, controlled grasping motions. Soft objects, like an orange (92.8 g), can be grasped, picked up and moved (Movie S 4). **(E)** The four BSPAs were also integrated as fingers in a soft pneumatic hand, together with a 6 cell prototype acting as a thumb. All actuators are controlled individually (Movie S 5).

were registered for 25.0 kPa. The low modulus (5.0 MPa) of the materials is the main factor for the softness of the grip. To validate the static elastic FEM-models in Abaqus (Fig. S 9) and the polymer characterization, the deformations and forces of the BSPAs were simulated as function of different overpressures and compared to the experimental results (Fig. 6 A, B, C). For both BSPA-designs, the experimental results agree very well with the simulation outcomes.

SH-soft pneumatic actuators in application

To validate the functionality of the SH-BSPAs, the four were used in a gripper application (Fig. 1B) as well as in a soft hand (Fig. 1 A, D). To control the actuator movement in these two applications, a setup was built in which 5 overpressures can be regulated individually using 5 control systems (Fig. S 14 and Fig. S 15). The soft pneumatic gripper was developed by placing the four bending actuators in a 3D printed part (Fig. 6D). The constructed gripper was subjected to tests gripping different soft items, including mandarin oranges, a rubber duck and cherry tomatoes (Fig. 6D). Using the control setup, the overpressure in the actuators can be regulated individually such that the force exerted by the four actuators on the soft object is almost identical at all times. A smooth, controlled grasping motion is created that allows picking up the different soft objects, as illustrated for the mandarin orange that weights 92.8 g (Movie S 4). These tests prove that the SH-BSPA and more specifically the DA-elastomers used possess an adequate flexibility and mechanical stability to be used in soft gripper applications.

In an alternative application, the BSPAs were placed together with a 6 cell prototype, created to act as a thumb, on a 3D printed part to form a soft pneumatic hand (Fig. 6E and Movie S 5). Because the actuators can be controlled individually, the soft hand can be used by a social robot to make gestures and to grasp soft objects. The soft actuators will ensure safe human-robot interactions in a dynamic, task-environment. The SH-capacity of the BSPA is validated further in the paper.

Design of the pneumatic artificial muscles

Different types of pneumatic artificial muscles have been developed, of which the McKibben muscle (*43*) is the most well-known. It contains an elastomeric inner membrane that will expand when inflated, through an elastic strain of the membrane, while a braided sleeving transfers tension. The expansion and contraction of the membrane displays hysteresis, which leads to a decrease in efficiency. In search of higher efficiencies, we developed pleated pneumatic artificial muscles (PPAM) (*37*, *44*), having a working principle that is different from others like the McKibben muscle (*43*). The membrane of the PPAM has a folded structure. In between the folds, cables are arranged that transfer tension. When pressurized, the muscle will expand and contract as a result of the unfolding of the pleats. Because the elastic deformation in PPAMs is limited, their efficiency is increased.

Because pneumatic muscles are usually constructed out of flexible membranes, wear, punctures or overpressures can damage the muscle and create leaks. In this study, we develop self-healing muscles by constructing the PPAM membrane using the flexible Diels-Alder polymers, such that damage can be healed using a mild heat treatment. Two prototypes (Fig. 7A and Movie S 6), PPAM 1 and PPAM 2 were elaborated in DPBM-FGE-J4000 and differ in the depth of the folds. The membrane has a thickness of 0.75 mm; the lengths of the PPAM 1 and PPAM 2, not including the fittings, are respectively 55 and 65 mm; and the muscles have a width of 36 and 33 mm (Specific dimensions in Fig. S 11). To transfer the tension, nylon cables were placed in between the folds. The manufacturing process that is used is again based on the shaping-through-folding-and-self-healing technique (Fig. S 13).

For the two designs, the deformation resulting from over

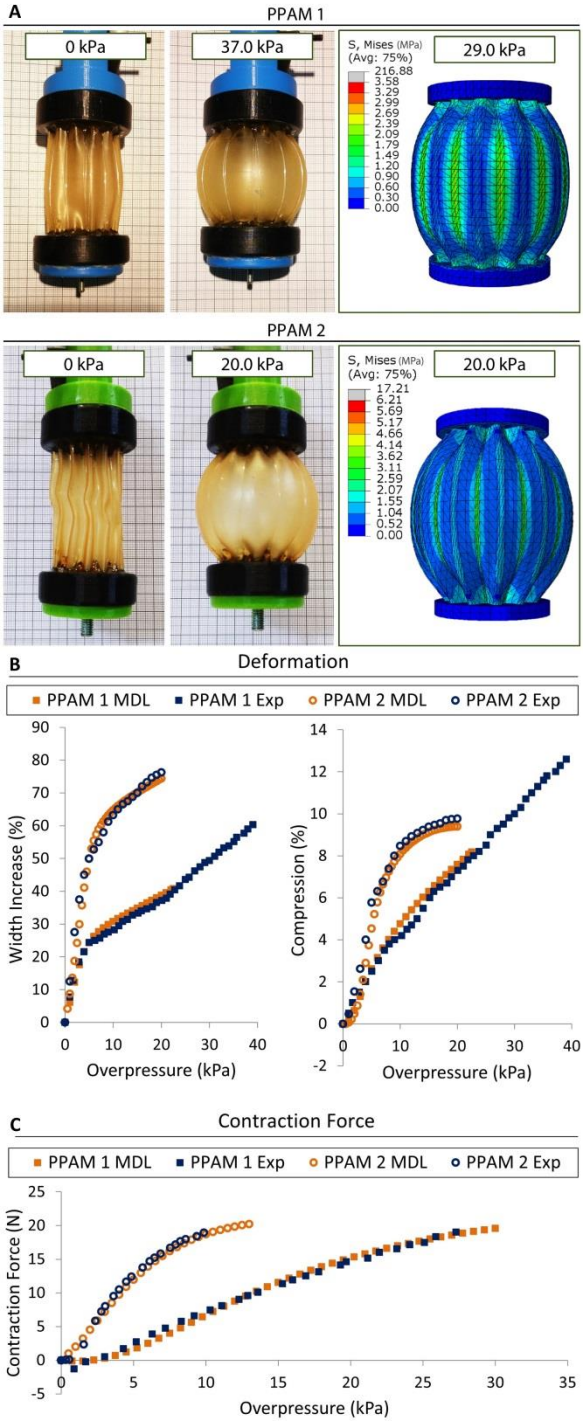

Fig. 7: Experimental deformations and contractions forces of the two PPAM designs, compared with the results of the numerical simulations using the static elastic model in Abaqus (Movie S 2). **(A)** Shape of the PPAM at ambient pressure and near maximum overpressure tested (Movie S 6). **(B)** Relative width increase and contraction as a function of the overpressure. **(C)** Contraction force as a function of the overpressure.

pressuring the muscle is simulated through a static elastic model in Abaqus (Fig. 7A, Fig. S 9 and Movie S 2). As for the BSPA, the simulation is limited to the elastic deformation response, modelled using the Young's modulus of the J4000-based DA-polymer (5.0 MPa) and the nylon cables (100 MPa). Gravity was accounted for (densities: J4000, 1.05 g/ml and nylon cables, 1.15 g/ml). The unfolding of the membrane as a result of applying an overpressure was captured using a digital camera (Fig. 7A and Movie S 6).

Mechanical properties of the pneumatic artificial muscles

The pressure in the muscles was regulated with the control system developed for the soft gripper and the soft hand (Fig. S 14 and Fig. S 15). The increase in relative width of the membrane and the relative contraction of the muscle were measured as a function of the overpressure. The deformation response consists of two phases. Already for low pressures the membrane starts to unfold and the width of the muscle and the contraction increase rapidly. At higher pressures, the membrane is entirely unfolded and the width increases slowly through the elastic straining of the membrane, increasing the contraction. Since the depth of the folds of PPAM 2 is bigger, the first phase results in larger deformations for similar overpressures. The small, negative force at very low pressures in PPAM 1 is due to the nylon cables that are not fully tightened, a problem that will be solved after the first healing cycle.

The contraction force was measured using a load cell (Futek LSB200, 15 lb), and is presented as a function of the overpressure in Fig. 7C. Forces up to 20 Newton were registered for pressures as low as 10.0 kPa. An additional advantage of the PPAM, compared to other pneumatic muscles like the McKibben, is that the response does not display a threshold pressure required for functioning (*37*, *44*, *45*). This makes them attractive for low pressure applications. As for the BSPAs, the deformations and the (contraction) forces of the PPAM designs were simulated using the static elastic Abaqus model (Fig. 7B). Again the experimental results coincide with the outcomes of the simulations for both designs. The operational properties of the two prototype PPAMs indicate that the Diels-Alder flexible self-healing polymers can be used to develop working pneumatic muscles with adequate performances for low pressure applications.

Self-healing of the actuators

The soft gripper, the soft hand and the two muscle prototypes demonstrate that the flexible DA-polymers have mechanical properties (Table 1) suitable for soft robotics. To evaluate the self-healing ability, cuts were made in the soft parts of the actuators using a scalpel blade with a thickness of 0.39 mm (Fig. 8 A, B). In future applications of the actuators in non-preprogramed, dynamic environments, they are more likely to be damaged when pressurized. This is the case for punctures and perforations due to high overpressures or wear, but also for damage caused by sharp items. When inflated, a pointy object can more easily slice through the membrane. For this reason, all the cuts were made when the actuators were inflated. When the actuator is inflated and a cut or perforation takes place, it will deflate and the pressure will drop. Thus, by checking the pressure needed to control a certain position, the health of the actuator can be monitored. If the damage is limited, the BSPAs and the PPAMs will to some degree keep working after being punctured, making them robust in use. However, the deformation and (contraction) force generate by the actuators depends on the pressure. Due to leaks the maximum pressure will decrease, reducing the deformation, force and contraction performances. More air mass will be consumed to compensate the leakage, increasing the energy consumption and hence decreasing the efficiency of the robot. Moreover, the pressure build-up will be slower and the dynamic performances will be reduced. Therefore, ability to self-heal is an important characteristic to restore the performances.

Because heating is required for the non-autonomous healing process, it can be performed at a desired time. A damaged actuator can for example still be active at lower efficiency for a limited time, after which it can be healed when the setup is put offline (e.g. at night). To initiate the healing process, the overpressure can be decreased to zero by the control system and the actuator can be completely deflated. In its non-inflated state, the soft pneumatic actuator has a self-sealing capacity: the formed cut or fracture surfaces will be naturally pressed together again, providing contact for the healing procedure. As long as the fracture surfaces are brought back in contact, healing is possible, however, if material is missing, this might no longer be feasible.

To confirm the SH-ability of the fingers of the soft pneumatic hand, cuts between 8 and 9.5 mm long were made in the inflated cell walls using a scalpel blade (Fig. 8A and Movie S 7). After applying damage, the actuator was deflated and the macroscopic cut was sealed autonomously. Subsequently the actuator was subjected to a heating procedure, in an oven (maximum temperature of 80 °C, detailed temperature profile in Fig. S 4). After this SH-procedure the damage was completely healed and the actuator was again airtight. The only thing that is left of the incident is a small scar on the surface of the cell wall due to microscopic misalignment of the fracture surfaces. A similar procedure was followed with the two PPAM prototypes. Again cuts of 8 to 9.5 were made with a scalpel blade in the soft membrane (Fig. 8B and Movie S 8). These could be healed by placing the muscles in the oven, which followed the same temperature profile (Fig. S 4). As for the BSPAs, all cuts could be healed entirely and only small superficial scars remained.

Besides sealing the damage, it is important that the mechanical properties of the actuators are recovered after the healing procedure. BSPA 3 was repeatedly damaged by cutting the tip cell with the scalpel blade (as in Fig. 8A: length of cuts between 8 and 9.5 mm) and healed using the procedure mentioned above (Fig. S 4). After each damage-healing procedure, the actuator was characterized again by measuring the bending deformation as a function of the overpressure in the cells. This damage-heal-measure cycle was repeated twice. Fig. 8C plots the bending angle as a function of the overpressure before healing, after 1 SH-cycle and after 2 SH-cycles. First of all, it can be noticed that

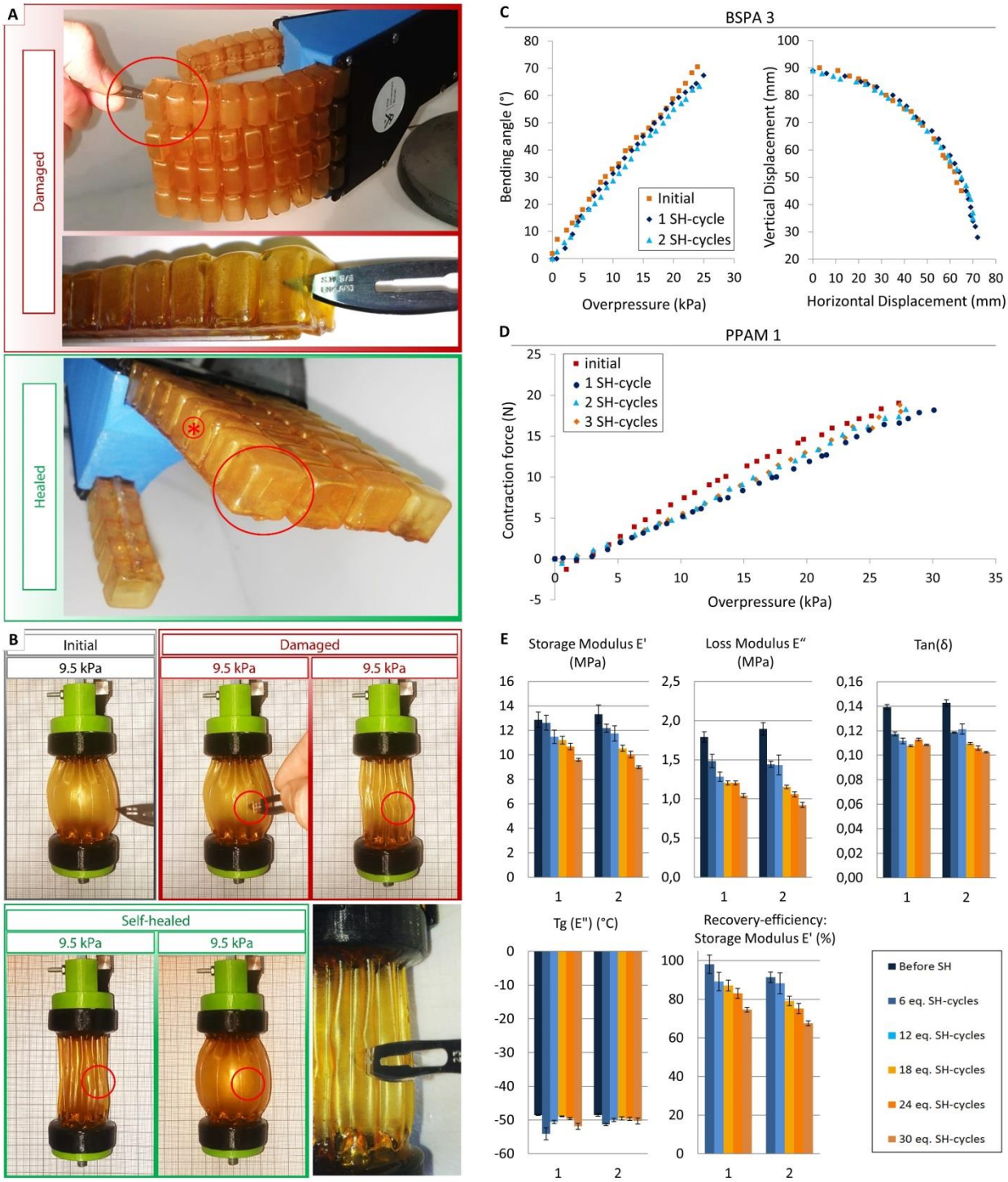

Fig. 8: Validating the SH-ability in practice: and recovery of the mechanical properties of the actuators after healing cuts, with lengths of 8 - 9.5 mm made with a scalpel blade**. (A)** Cutting the finger actuator (BSPA) with a scalpel blade with a thickness of 0.39 mm (Movie S 7). The macroscopic cuts (length 9.4 mm and all the way through) can be healed entirely using a SH-procedure, after which the actuator is again completely airtight. The star indicates the location of failure due to overpressure. **(B)** Macroscopic cuts (8.6 mm) in the self-healing membrane of the PPAM can be healed entirely using a SH-procedure (Movie S 8). After this the muscle is again airtight and recovers its functionality. **(C)** The bending angle as a function of overpressure and the trajectory of the tip of the BSPA are measured after 1 and 2 damage-SH-cycles and are compared with the initial characteristics. **(D)** Contraction force of the PPAM 1 as a function of overpressure as measured after 1, 2 and 3 damage-SH-cycles and compared with the initial characteristics. **(E)** Influence of the heating procedure (4 hours at 80°C followed by at least 3 days at 25°) on the visco-elastic properties expressed in equivalent SH-cycles.

repeatedly healing damages using the heating procedure does not influence the actuators trajectory: the results are very similar and taking in account minimal variations in the position of the actuator in the test setup, it can be concluded that the mechanical properties of the bending actuator were recovered after each SH-cycle.

After the first damage-heal-measure cycle, the BSPA 3 was pushed to its limits by gradually increasing the overpressure. The actuator failed at 24.2 kPa, but not at the location of the scar. A perforation took place on the side of one of the cells (indicated with (*) in Fig. 8A). Also this new perforation was sealed and made airtight using the SH-procedure. Upon pressurizing until failure after the second damage-heal-measure cycle, the BSPA failed at 25.0 kPa, at a third location, on the side of another cell. From these tests it can concluded that no weak spots are created on the location of scars and healed perforations.

To validate the recovery of the properties of the self-healing artificial muscles, PPAM 1 was repeatedly damaged by making a cut all the way through the membrane with the scalpel blade (Fig. 8B) and healed for 3 times in total. After each healing process, the isometric contraction force was measured as a function of the overpressure in the muscle (Fig. 8D) and compared to the characterization curve of the undamaged PPAM. After the first damage-heal cycle the characterization curve shifted somewhat downwards. This is due to a slight deformation of the membrane because the muscle was manufactured horizontally but healed vertically in the oven. Because this was done vertically, the nylon cables are tightened, which can be seen in a loss of the negative threshold pressure, seen in the initial curve. Between the first, second and third cycle there is only a slight variation in the curves. The curve moves slightly up with every damage-heal cycle, due to a minor change in material properties explained in the next section.

Self-healing efficiency

The influence of the heating procedure on the mechanical properties of the DA-polymer and their repeated recovery was examined. To do so, 6 series of each 4 samples for two different batches of the J4000-based DA-polymer were prepared. All samples, except the reference series, were subjected to a heating procedure (4 hours at 80 °C followed by at least 3 days at 25 °C), which can be considered the equivalent of 6 SH-procedures based on the isothermal step (Fig. 3) that has a duration of 40 min (Fig. S 4). For one series, this heating procedure was performed once, for the next twice, for the third three times, etc., giving an equivalent of 0, 6, 12, 18, 24 and 30 SH-cycles. For each series, Dynamic Mechanical Analysis (DMA) was used to measure storage modulus, loss modulus, tan (δ) and the glass transition temperature (Fig. 8E).

From Fig. 8E, it is clear that for every 4 hours spent at 80 °C, the equivalent of 6 SH-cycles, the storage modulus, the loss modulus and tan(δ) lower a bit, while the glass transition temperature remains more or less the same. The reproducibility of the observed decreasing trends was proven by the similarity between the results of batch 1 and 2. The small drop might point to a limited decrease in cross-link density resulting from the formation of irreversible bonds through two side reactions in the network: the Michael addition of amine impurities to maleimide groups and the homopolymerization of bismaleimide, both occurring at higher temperatures (Fig. S 16). These side reactions imply that some of the furan functionalities can no longer form a Diels-Alder bond, resulting in a gradual decrease of the cross-link density and modulus after healing. The recovery efficiency, defined as $(E'_{initial}-E'_{xSH\text{-}cyles})/(E'_{initial})$ is on average 93.4 % for one 4-hour heating cycle (Fig. 8E). Projecting this on a 1-hour SH-cycle, a high recovery efficiency of 98-99 % is reached. The small increase in flexibility results in the small increase in the contraction force of the PPAM actuator observed for 2nd and 3rd SH-cycles (Fig. 8E). We believe that the Michael addition has the largest influence, since this reaction occurs at lower temperatures compared to the homopolymerization. The recovery efficiency can be increased by working with a bismaleimide with higher purity and by avoiding the presence of unreacted amine, reducing the Michael addition.

Recycling of the self-healing material

To illustrate the recyclability of the DA- polymers, cells that could be used in a BSPA (as in Fig. 4D), were cut into pieces, and subsequently dissolved in $CHCl_3$ (Fig. S 17). Indeed, swelling and further dilution decrease the concentration of the DA-adduct, gradually shifts the equilibrium to the unbound state. To accelerate the dissolution step, the temperature was raised to 65 °C. The obtained solution could be solvent-cast into a sheet again. Similar to the SH-procedure, the recycling procedure involved a heating step during solvent-casting. Therefore, a slight drop in storage modulus (E' = 10.5 MPa) compared to the initial properties (E' = 12.9 MPa) is displayed, resulting in a recovery efficiency of 81 % (more details in Fig. S 18). This change in properties can be reduced if bismaleimide is used with higher purity. The recycled sheet (Fig. S 17) was used to manufacture parts of the 6-cell bending soft pneumatic actuator; the thumb of the soft hand. This proves that the SH-soft robotic parts can be recycled.

Discussion

The use of flexible material in robotics opens up new opportunities: soft robotics can perform tasks in uncertain, dynamic environments, without the need of extensive control systems. Their intrinsic softness makes them ideal for safe interactions with their surroundings, which can include people. However, softness and flexibility also imply an increased vulnerability to all kinds of sharp objects and edges found in the uncertain environments in which these robots will function, which is also valid for soft organisms, as a matter of fact. However, if an organism's injuries are limited and given time, they can recover from their injuries. This work has successfully introduced a similar healing ability in soft robotics, more specifically in soft pneumatic actuators. Flexible Diels-Alder (DA) self-healing (SH) polymers, consisting of a thermoreversible covalent network, were synthesized and used to manufacture prototypes for three different self-healing soft robotic applications: a soft gripper, a soft hand and artificial muscles.

The healing action of these DA-polymers can be activated by means of a mild heat stimulus. Macroscopic damage in DA-sheets, such as mm-long cuts all the way through, made with a scalpel blade, can be successfully healed by heating the parts to 80 °C for 40 min and slowly cooling down to 25 °C (-2 $K.min^{-1}$). After 24 hours at 25 °C, the initial properties are almost entirely recovered. In the synthesis phase, the mechanical properties can be tuned to fit a wide variety of properties desired for different robotic applications. In this work, a series of three polymers was

synthesized that differs in spacer length and resulting mechanical properties. However, many other variations are feasible. As their SH-ability is based on the same reversible DA-crosslinks in their network structures, sheets or parts with completely different mechanical properties can be seamlessly healed together, which can be beneficial in the soft robotics manufacturing process. The mechanical characterization of the flexible DA-polymers displays properties adequate for soft robotics applications.

The most flexible polymer of the DA-series, DPBM-FGE-J4000, was used in our current SH-soft robotic applications. For all three soft pneumatic systems, the soft gripper, the soft hand and the artificial muscles, the design was supported by simulating large deformations using a static elastic finite element model (FEM) in Abaqus. To build the prototypes, a manufacturing process involving folding and self-healing was developed, which exploits the SH-ability of the DA-polymers. Flexible DA-sheets are first folded into 3D polygon structures. The creases can be made permanent and the joints airtight by subjecting the part to a mild heating procedure (< 80 °C globally and < 110 °C locally). Using this technique, soft actuators such as the fingers of the soft hand can be made as a single part and almost entirely out of SH-material.

The performance of the SH-prototypes was experimentally validated using dedicated test benches that contain pressure regulating systems, a digital camera, and force and pressure sensors. The measured performance, deformations and forces resulting from pressurizing the membrane, are adequate for soft robotic applications and coincide with the results from the FEM-simulations. The SH-capacity of the prototypes was verified by healing realistic macroscopic damage applied to the membrane. Using a scalpel blade relatively large cuts were made all the way through the membranes of the pressurized actuators. Because of the self-sealing ability of the pneumatic actuator in non-inflated condition, the cut surfaces are naturally pressed together. When subjected to a SH-procedure (max temp 80 °C), all cuts were healed, leaving nothing but a small scar behind (due to microscopic misalignment). At the location of the scar, the membrane was again airtight and no weak spots were created.

It is crucial that after the healing operation, the performance of the actuator is recovered. For this reason the actuators were repeatedly damaged, healed and tested, showing that the performance is almost entirely restored. There is only a very small change for the PPAM actuators, due to a slight increase in the flexibility of the DA-elastomers after each healing cycle. The storage modulus of the flexible DA-polymer is recovered with 98-99 %. As slow side reactions are thought to be at the origin, in casu the maleimide homopolymerization, this recovery efficiency might be increased by utilizing bismaleimide with higher purity in the synthesis and avoiding tertiary amines that catalyse the homopolymerization.

An additional advantage of the DA-polymers is that they are recyclable, either by remoulding them, or by dissolving them in a suitable solvent. 3D polygon waste structures of the DA-polymer were cut into small pieces and subsequently dissolved. Through solvent-casting, recycled sheets could be created, with a recovery efficiency of the storage modulus of 81 %, an efficiency that might again be increased by reducing the occurrence of side reactions using bismaleimides with a higher purity. Recycled sheets were used to manufacture the thumb of the soft hand. Therefore, DA-polymers have potential to support an ecological transfer from lab-setting to an industrial scale and to our daily environment.

This study, illustrates through demonstrators that self-healing Diels-Alder elastomers can be used for a variety of soft robotic applications. Because of SH-capacity given to the actuators, different types of damage to the membranes can be healed using mild heating procedures. This SH-principle increases the life span of soft robotic components while their over-dimensioning, previously used to withstand damaging conditions, can be reduced.

Materials and Methods

Reagents

Furfuryl glycidyl ether (FGE, 96 %) and 1,1'-(methylenedi-1,4-phenylene)bismaleimide (DPBM, 95%) were obtained from Sigma-Aldrich (Fig. S 1). The Jeffamine D-series (poly(propylene glycol) bis(2-aminopropyl ether) with average degree of polymerization n (as determined by NMR) were obtained from Huntsman and have following characteristics: J400: $n = 6.9$, $M_n = 477$ g.mol^{-1}; J2000: $n = 44.2$, $M_n = 2640$ g.mol^{-1}; J4000: $n = 71.1$, $M_n = 4200$ g.mol^{-1}. Chloroform (stab./Amylene) (min 99.9%) was obtained from Biosolve Chimie. All chemicals were used as delivered.

Synthesis of the DA-polymers

FGE is reacted with a stoichiometric amount of Jeffamine Jx (x = 400, 2000, or 4000), yielding a furan-functionalized compound with functionality 4 (FGE-Jx). This reaction was performed at 60 °C for minimum 7 days under continuous stirring, after which the reaction was completed at 90 °C for 2 days. The functionality of the FGE-Jx compound was 4.0 ± 0.2, as checked by NMR. To produce the DA-polymers (details in Fig. S 1), the furan-functionalized compound (FGE-Jx) was mixed with DPBM in a stoichiometric ratio ($r = n_{Maleimide}/n_{Furan} = 1$) and dissolved in chloroform (20 w% solution). To ensure complete dissolution of the DPBM in chloroform, the mixture was stirred at 25 °C for 24 hours. To form sheets of the thermoreversible networks, the solution is casted in Teflon moulds, and the chloroform is evaporated. The chloroform is evaporated by increasing the temperature up to 90 °C under vacuum. The thermo-reversible network is formed by slowly cooling down the sheet after the chloroform has been evaporated completely.

Measuring of the mechanical behaviour

The visco-elastic behaviour of the DA-polymer networks DPBM-FGE-J400, -J2000 and -J4000, were measured on a TA Instruments Q800 DMA for 3 to 4 samples per material. Rectangular samples of 0.2-0.7 mm thick, 1.5-3.2 mm wide, and 3.6-4.6 mm long were measured in tension mode at a frequency of 1 Hz, oscillation strain of 0.1 %, and force tracking of 125 % and using a heating rate of 10 K.min^{-1} (Fig. S 5). The glass transition temperature is taken as the temperature where the loss modulus reaches its maximum.

The fracture strain and stress of the different polymers of the DA-series were measured 25 °C using stress-strain tests until fracture (Fig. S 6). The measurements were performed on a TA Instruments Q800 DMA in controlled strain mode with rectangular samples in tension for 4 samples per materials. For the glassy J400-based material, a rate of 0.1 %.min^{-1} was used, while for the elastomeric J2000- and

J4000-based materials a rate of 65 %.min^{-1} was used. The samples had a thickness of 0.2-0.7 mm, a width of 1.7-5.5 mm, and a length of 4.0-4.2 mm, adjusted to the mechanical behaviour of the materials. The Young's modulus, was obtained from a stress-strain curve with a strain ramp of 65 %.min^{-1} for the J2000- and J4000-based materials and 0.1 %.min^{-1} for the J400, using a linear regression over the strain interval (J4000: 0%-5%; J2000: 0%-2.5%; J400: 0%-0.2%)(Fig. S 7).

Temperature profile of the SH-process

The SH-procedure used in practice to heal the damage to the actuators consists out of 4 phases (Fig. S 4): the sample is placed in an oven at 80 °C where it is heated at about 10 K.min^{-1} to 80 °C and it is kept isothermal for about 35 min. Subsequently, the sample is cooled at about 2 K.min^{-1} to 25 °C, where it is kept about 24 h to fully restore the mechanical properties. The temperature profile was optimized using kinetic simulations (Fig. S 3).

Pressure controlling system

In the setup 5 pressures can be regulated by 5 control systems in parallel (Fig. S 14 and Fig. S 15). Each system contains a buffer volume and two solenoid valves (Matrix 720 Series compact): one connected to a pressure source, and the other to atmospheric pressure. These are switched at high frequency using PWM controlled Power FET Switches (MOSFET 4 v04). The PWM signal is provided by an Arduino Mega ADK board. The pressure signal is measured using a Honeywell Differential Pressure Sensor (15 psi, 10 V dc) and amplified using an instrumentation amplifier of Analog Devices, AD623ANZ. For the force measurements a two different load cells were used FUTEK LSB200 2 lb and 50 lb. Their signals were amplified using the FUTEK Amplifier Module CSG110.

Supplementary Material

Fig. S 1: Synthesis of the thermoreversible covalent networks.
Fig. S 2: The thermoreversible Diels-Alder reaction.
Fig. S 3: Simulation for the DA-series: DPBM-FGE-J400, DPBM-FGE-J2000 and DPBM-FGE-J4000.
Fig. S 4: Temperature profile of the self-healing procedure.
Fig. S 5: Temperature dependent visco-elastic behaviour for the DA-polymer series measured by DMA.
Fig. S 6: Stress strain curves for the DA-polymer series.
Fig. S 7: Young's Modulus determination of the DPBM-FGE-Jx
Fig. S 8: Measuring the gel temperature (Tgel) through dynamic rheometry.
Fig. S 9: Simulating different designs for the self-healing soft robotic demonstrators using a static elastic model in Abaqus.
Fig. S 10: Dimensions of the two BSPA designs in mm.
Fig. S 11: Dimensions of the two PPAM prototypes in mm.
Fig. S 12: Constructing a BSPA using "shaping-through-folding-and-self-healing".
Fig. S 13: "Shaping-through-folding-and-self-healing" to manufacture the PPAMs.
Fig. S 14: Pressure control system scheme.
Fig. S 15: Images of the pressure control system.
Fig. S 16: Irreversible crosslinking of bismaleimide networks.
Fig. S 17: Diels-Alder polymer waste of the manufacturing process of the prototypes can be recycled.
Fig. S 18: Recovery of the material properties after the recycling procedure.

Movie S 1: The visualization of the self-healing process of the Diels-Alder elastomers, using optical microscopy.
Movie S 2: Healing Diels-Alder polymers together with different mechanical properties; DPBM-FGE-J4000 and DPBM-FGE-J2000.
Movie S 3: Simulating large deformations using static elastic models in Abaqus.
Movie S 4: The soft pneumatic gripper handling a 92 g mandarin orange.
Movie S 5: The soft pneumatic hand, in which all the fingers are controlled individually.
Movie S 6: The actuation of the pleated pneumatic artificial muscle.
Movie S 7: Damaging the soft pneumatic hand.
Movie S 8: Damaging the pleated pneumatic artificial muscles.

References

1. C. Laschi, B. Mazzolai, M. Cianchetti, Soft robotics : Technologies and systems pushing the boundaries of robot abilities. *Sci. Robot.* **3690**, 1–11 (2016).

2. S. Kim, C. Laschi, B. Trimmer, Soft robotics: a bioinspired evolution in robotics. *Trends Biotechnol.* **31**, 287–294 (2013).

3. D. Rus, M. T. Tolley, Design, fabrication and control of soft robots. *Nature*. **521**, 467–475 (2015).

4. D. Trivedi, C. D. Rahn, W. M. Kier, I. D. Walker, Soft robotics: Biological inspiration, state of the art, and future research. *Appl. Bionics Biomech.* **5**, 99–117 (2008).

5. R. H. Ewoldt, Extremely Soft: Design with Rheologically Complex Fluids. *Soft Robot.* **1**, 12–20 (2014).

6. M. T. Tolley *et al.*, A Resilient, Untethered Soft Robot. *Soft Robot.* **1**, 213–223 (2014).

7. S. A. Morin *et al.*, Camouflage and Display for Soft Machines. *Science*. **337**, 828–832 (2012).

8. R. F. Shepherd *et al.*, Multigait soft robot. *Proc. Natl. Acad. Sci.* **108**, 20400–20403 (2011).

9. R. Deimel, O. Brock, A Novel Type of Compliant and Underactuated Robotic Hand for Dexterous Grasping. *Int. J. Rob. Res.* **35**, 161–185 (2015).

10. E. Brown *et al.*, Universal robotic gripper based on the jamming of granular material. *Proc. Natl. Acad. Sci.* **107**, 18809–18814 (2010).

11. S. Wakimoto, K. Ogura, K. Suzumori, Y. Nishioka, Miniature soft hand with curling rubber pneumatic actuators. *2009 IEEE Int. Conf. Robot. Autom.*, 556–561 (2009).

12. J. Hughes *et al.*, Soft Manipulators and Grippers: A Review. *Front. Robot. AI.* **3**, 1–12 (2016).

13. J. Amend, H. Lipson, The JamHand : Dexterous Manipulation with Minimal Actuation. *Soft Robot.* **4**, 70–80 (2017).

14. R. V. Martinez, A. C. Glavan, C. Keplinger, A. I. Oyetibo, G. M. Whitesides, Soft Actuators and Robots

that Are Resistant to Mechanical Damage. *Adv. Funct. Mater.* **24**, 3003–3010 (2014).

15. S. Terryn *et al.*, Development of a self-healing soft pneumatic actuator: a first concept. *Bioinspir. Biomim.* **10**, 046007 (2015).

16. S. R. White *et al.*, Autonomic healing of polymer composites. *Nature*. **409**, 794–797 (2001).

17. X. Chen *et al.*, A thermally re-mendable cross-linked polymeric material. *Science*. **295**, 1698–702 (2002).

18. D. Y. Wu, S. Meure, D. Solomon, Self-healing polymeric materials: A review of recent developments. *Prog. Polym. Sci.* **33**, 479–522 (2008).

19. B. J. Blaiszik *et al.*, Self-Healing Polymers and Composites. *Annu. Rev. Mater. Res.* **40**, 179–211 (2010).

20. S. D. Bergman, F. Wudl, Mendable polymers. *J. Mater. Chem.* **18**, 41–62 (2008).

21. M. D. Hager, P. Greil, C. Leyens, S. van der Zwaag, U. S. Schubert, Self-healing materials. *Adv. Mater.* **22**, 5424–30 (2010).

22. A. Lutz *et al.*, A Shape-Recovery Polymer Coating for the Corrosion Protection of Metallic Surfaces. *ACS Appl. Mater. Interfaces*. **7**, 175–183 (2014).

23. H. Jonkers, Self healing concrete: a biological approach. *Self Heal. Mater.*, 195–204 (2008).

24. K. L. Gordon, R. K. Penner, P. B. Bogert, W. T. Yost, E. J. Siochi, Puncture Self-Healing Polymers for Aerospace Applications. *Conf. NASA Am. Chem. Soc. Natl. Meet. Expo.* **242**, NF1676L–12452 (2011).

25. B. C. Tee, C. Wang, R. Allen, Z. Bao, An electrically and mechanically self-healing composite with pressure-and flexion-sensitive properties for electronic skin applications. *Nat. Nanotechnol.* **7**, 825–832 (2012).

26. C. Hou *et al.*, A strong and stretchable self-healing film with self-activated pressure sensitivity for potential artificial skin applications. *Sci. Rep.* **3**, 3138–3142 (2013).

27. M. Yim *et al.*, Modular Self-Reconfigurable Robot Systems [Grand Challenges of Robotics]. *Robot. Autom. Mag.* **14**, 43–52 (2007).

28. Y.-L. Liu, T.-W. Chuo, Self-healing polymers based on thermally reversible Diels–Alder chemistry. *Polym. Chem.* **4**, 2194 (2013).

29. B. Scheltjens, Gill, Diaz, M. M., Brancart, Joost, Van Assche, Guy, Van Mele, Thermal evaluation of a self-healing polymer network coating based on reversible covalent bonding. *React. Funct. Polym.* **73** (2013).

30. B. Ghosh, M. W. Urban, Self-Repairing Oxetane-Substituted. *Science*. **323**, 1458–60 (2009).

31. P. Cordier, F. Tournilhac, C. Soulié-Ziakovic, L. Leibler, Self-healing and thermoreversible rubber from supramolecular assembly. *Nature*. **451**, 977–80 (2008).

32. J. Saldien, K. Goris, B. Vanderborght, J. Vanderfaeillie, D. Lefeber, Expressing Emotions with the Social Robot Probo. *Int. J. Soc. Robot.* **2**, 377–389 (2010).

33. P. Polygerinos *et al.*, Towards a Soft Pneumatic Glove for Hand Rehabilitation. *Proc. IEEE/RSJ Int. Conf. Intell. Robot. Syst.*, 1512–1517 (2013).

34. A. D. Marchese, R. K. Katzschmann, D. Rus, A Recipe for Soft Fluidic Elastomer Robots. *Soft Robot.* **2**, 7–25 (2015).

35. B. Mosadegh, Pneumatic networks for soft robotics that actuate rapidly. *Adv. Funct. Mater.* **24**, 2163–2170 (2014).

36. http://www.softroboticsinc.com/.

37. D. Villegas, M. Van Damme, B. Vanderborght, P. Beyl, D. Lefeber, Third-Generation Pleated Pneumatic Artificial Muscles for Robotic Applications: Development and Comparison with McKibben Muscle. *Adv. Robot.* **26**, 1205–1227 (2012).

38. B. Vanderborght, R. Van Ham, B. Verrelst, M. Van Damme, D. Lefeber, Overview of the Lucy Project: Dynamic Stabilization of a Biped Powered by Pneumatic Artificial Muscles. *Adv. Robot.* **22**, 1027–1051 (2008).

39. S. Terryn *et al.*, Toward Self-Healing Actuators: A Preliminary Concept. *IEEE Trans. Robot.* **32**, 736–743 (2016).

40. S. Terryn *et al.*, Investigation of self-healing compliant actuators for Robotics. *IEEE Int. Conf. Robot. Autom.*, 258–263 (2015).

41. F. Ilievski, A. D. Mazzeo, R. F. Shepherd, X. Chen, G. M. Whitesides, Soft Robotics for Chemists. *Angew. Chemie*. **123**, 1930–1935 (2011).

42. Y. Sun, Y. Seong Song, J. Paik, Characterization of silicone rubber based soft pneumatic actuators. *Proc. IEEE/RSJ Int. Conf. Intell. Robot. Syst.*, 4446–4453 (2013).

43. G. K. Klute, B. Hannaford, Accounting for Elastic Energy Storage in McKibben Artificial Muscle Actuators. *J. Dyn. Syst. Meas. Control*. **122**, 386–388 (2000).

44. B. Verrelst, R. Van Ham, Second generation pleated pneumatic artificial muscle and its robotic applications. *Adv. Robot.* **20**, 783–805 (2006).

45. F. Daerden, D. Lefeber, The concept and design of pleated pneumatic artificial muscles. *Int. J. Fluid Power*. **2**, 41–50 (2001).

Funding: This research is funded by the European Commission ERC Starting grant SPEAR (no.337596). S. Terryn is funded by PhD Fellowship of the Research Foundation Flanders (FWO). **Author contributions:** S. Terryn designed and performed all experiments; J. Brancart assisted in characterizing the Diels-Alder polymers; all authors contributed in the writing of the paper. **Data and materials availability:** All data supporting conclusions can be found in supplementary materials. For more detailed information on materials and methods contact S. Terryn (seterryn@vub.ac.be).

SUPPLEMENTARY MATERIALS

Synthesis of the Diels-Alder polymers

The reactants used in the synthesis of the reversible DA-polymer network system are depicted in Fig. S 1:

ˆ (A): 3 Jeffamine D-series: poly(propylene glycol) bis(2-aminopropyl ether) with average degree of polymerization n (determined by NMR spectroscopy) (obtained from Huntsman)

- J400: n = 6.9, Mn = 477 g/mol
- J2000: n = 44.2, Mn = 2640 g/mol
- J4000: n = 71.1, Mn = 4200 g/mol

ˆ (B): furfuryl glycidyl ether (FGE, 96 %) (obtained from Sigma-Aldrich)

(C): 1,1'-(methylenedi-1,4-phenylene)bismaleimide (DPBM, 95%) (obtained from Sigma-Aldrich)

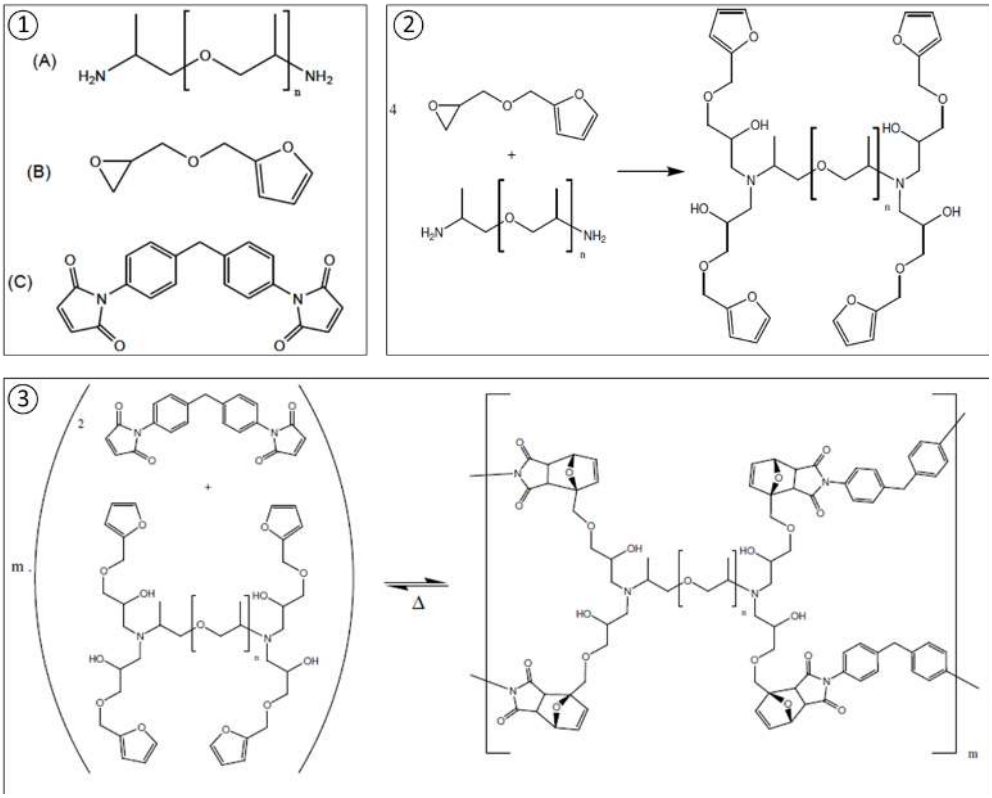

Fig. S 1: Synthesis of the thermoreversible covalent networks: (1) Reagents used in the synthesis: A) Jeffamine, B) furfuryl glycidyl ether and C) Bismaleimide. **(2)** The irreversible epoxy-amine reaction between Jeffamine and furfuryl glycidyl ether giving the furan-functionalized building block with selected spacer length. **(3)** The creation of the network as a result of the formation of crosslinks by the Diels-Alder reaction between maleimide and furan groups.

Step 1: Fig. S 1.2: FGE mixed with a stoichiometric amount of Jeffamine Jx (x = 400, 2000, and 4000) through an epoxy-amine reaction, yielding a furan-functionalized compound (FGE-Jx). This reaction was performed at 60 °C for minimum 7 days under continuous stirring, after which the reaction was completed at 90 C° for 2 days.

Step 2: Fig. S 1.3: The furan-functionalized compound (FGE-Jx) was mixed with DPBM in a stoichiometric ratio (r= $n_{Maleimide}$ / n_{Furan} = 1) and dissolved in chloroform (20 w% solution). To ensure complete dissolution of the DPBM in chloroform, the mixture was stirred at 25°C for 24 hours.

Step 3: To form sheets of the thermoreversible networks, the solution is casted in Teflon moulds, and the chloroform is evaporated. The chloroform is evaporated by increasing the temperature up to 90 °C under vacuum. The thermoreversible network is formed by slowly cooling down the sheet after the chloroform has been completely evaporated. The detailed evaporation and cooling procedure goes as follows:

I) 1 hour at 60°C and decrease pressure to 60.0 kPa. II) Gradually increase the temperature to 90 °C (0.5 $K.min^{-1}$). III) Gradually decrease the pressure up to vacuum of 0 kPa. IV) Keep at 90°C and vacuum until all gas bubbles are removed. The material is liquid at this moment. V) Cool down at about 2 $K.min^{-1}$ to 25 °C, remaining under vacuum. VI) Leave the sheet for 24 days at 25°C and under vacuum.

Simulating the equilibrium and the kinetics of the Diels-Alder reaction

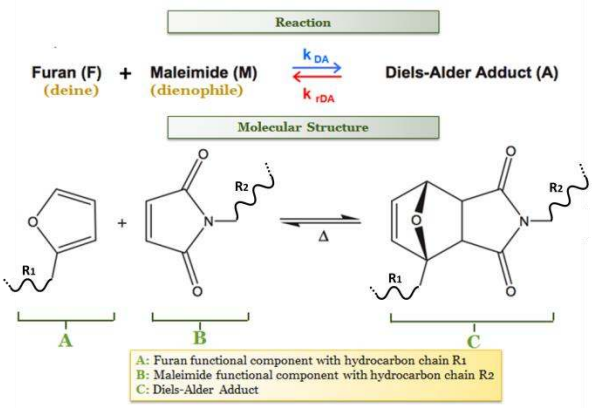

Fig. S 2: The thermoreversible Diels-Alder reaction.

Both the temperature dependence of the equilibrium conversion and the time- and temperature-dependent kinetics of the reversible Diels-Alder reaction between DPBM, the maleimide-carrying group, and FGE-Jeffamine, the furan-carrying group, were modelled.

The equilibrium equation:

The equation for the equilibrium constant is given by:

$$\text{Eq. 1: } \boldsymbol{K} = \frac{\boldsymbol{k_{DA}}}{\boldsymbol{k_{rDA}}} = \frac{[\boldsymbol{A}]_{\boldsymbol{eq}}}{[\boldsymbol{F}]_{\boldsymbol{eq}}[\boldsymbol{M}]_{\boldsymbol{eq}}}$$

with $[F]_{eq}$, $[M]_{eq}$ and $[A]_{eq}$ the molar concentrations of furan, maleimide and Diels-Alder adduct at equilibrium.

Starting from the initial concentrations $[F]_0$, $[M]_0$ and $[A]_0$ for which we take $[M]_0 = [F]_0$ and $[A]_0 = 0$ for the stoichiometric conditions used in this work, we can write all concentrations as a function of the conversion at equilibrium:

$$\text{Eq. 2: } [\mathbf{M}]_{\boldsymbol{eq}} = [\mathbf{F}]_{\boldsymbol{eq}} = [\mathbf{F}]_{\mathbf{0}}(\mathbf{1} - \boldsymbol{x_{eq}}) \qquad [\mathbf{A}]_{\boldsymbol{eq}} = [\mathbf{F}]_{\mathbf{0}}(\boldsymbol{x_{eq}})$$

The rate constants k_{DA} and k_{rDA}, which are a function of temperature, are given by Arrhenius equations Eq. 3, with A_{DA} and A_{rDA} the pre-exponential factors, E_{DA} and E_{rDA} the activation energies, R the universal gas constant, and T the absolute temperature**:**

$$\text{Eq. 3: } \boldsymbol{k_{DA}} = \boldsymbol{A_{DA}} e^{\frac{-E_{DA}}{RT}} \text{ and } \boldsymbol{k_{rDA}} = \boldsymbol{A_{rDA}} e^{\frac{-Er_{DA}}{RT}}$$

Substituting Starting from the initial concentrations $[F]_0$, $[M]_0$ and $[A]_0$ for which we take $[M]_0 = [F]_0$ and $[A]_0 = 0$ for the stoichiometric conditions used in this work, we can write all concentrations as a function of the conversion at equilibrium:

Eq. 2 in Eq. 1 and rearranging leads to the following expression for the equilibrium conversion:

$$\text{Eq. 4: } \boldsymbol{x_{eq}} = \frac{(2\boldsymbol{K}[\boldsymbol{F}]_0+1)-\sqrt{4\boldsymbol{K}[\boldsymbol{F}]_0+1}}{2\boldsymbol{K}[\boldsymbol{F}]_0}$$

The kinetics equation:

At any instant, the rate of consumption for maleimide can be written as:

$$\text{Eq. 5: } -\frac{\boldsymbol{d}[\boldsymbol{M}]}{\boldsymbol{dt}} = -\frac{\boldsymbol{d}[\boldsymbol{F}]}{\boldsymbol{dt}} = \frac{\boldsymbol{d}[\boldsymbol{A}]}{\boldsymbol{dt}} = \boldsymbol{k_{DA}}[\boldsymbol{F}][\boldsymbol{M}] - \boldsymbol{k_{rDA}}[\boldsymbol{A}]$$

As for the equilibrium equation, we can rewrite the concentrations as a function of the reaction conversion x, assuming a stoichiometric system:

$$\text{Eq. 6: } [\mathbf{M}](\boldsymbol{t}) = [\mathbf{F}](\boldsymbol{t}) = [\mathbf{F}]_{\mathbf{0}}(\mathbf{1} - \boldsymbol{x}(\boldsymbol{t})) \qquad [\mathbf{A}](\boldsymbol{t}) = [\mathbf{F}]_{\mathbf{0}}(\boldsymbol{x}(\boldsymbol{t}))$$

As for the equilibrium equation, we can rewrite the concentrations as a function of the reaction conversion x, assuming a stoichiometric system:

Eq. 6 can be substituted in this At any instant, the rate of consumption for maleimide can be written as:

Eq. 5. After rearranging this leads to the following rate equation for the DA-reaction:

$$\text{Eq. 7: } \frac{\boldsymbol{dx}(\boldsymbol{t})}{\boldsymbol{dt}} = \boldsymbol{k_{DA}}[\boldsymbol{F}]_0(\mathbf{1} - \boldsymbol{x}(\boldsymbol{t}))^2 - \boldsymbol{k_{rDA}}\boldsymbol{x}(\boldsymbol{t})$$

Using equations Eq. 4 and Eq. 7 both the equilibrium and non-equilibrium conversions can be modelled (Fig. S 3). Using the equilibrium reaction Fig. S 3A, the equilibrium conversion for every temperature can be calculated and plotted. Using the kinetics simulation Fig. S 3B, we can calculate how long it will take to reach this equilibrium conversion for a certain temperature profile which is followed. This simulation can be used to calculate how long it will take before the mechanical

properties of the Diels-Alder polymer, DPBM-FGE-J4000, are recovered (at equilibrium) after the cooling step of the SH-procedure. For the cooling step used in the SH-procedure, from 80 °C to 25 °C with a rate of -2 $Kmin^{-1}$, the evolution of the conversion follows the blue graph in Fig. S 3B. After the cooling ramp the material has to remain at 25 °C for 22.24 hours in order to reach 97.5% of the equilibrium conversion and recover its mechanical properties. Through this simulation the temperature profile of the practical healing procedure (next section) was determined.

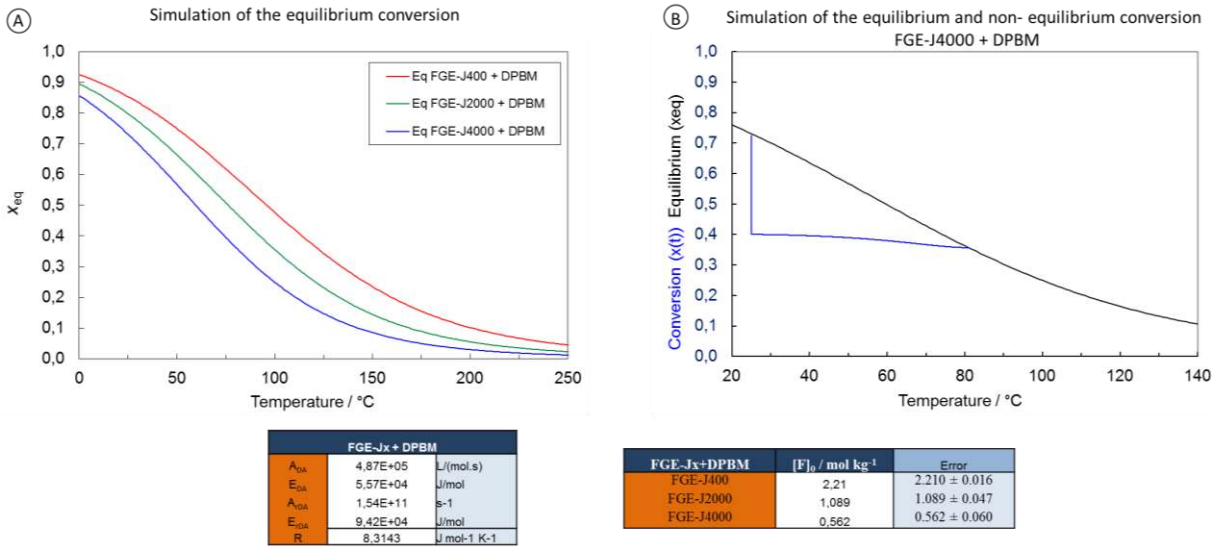

FGE-Jx + DPBM		
A_{DA}	4,87E+05	L/(mol.s)
E_{DA}	5,57E+04	J/mol
A_{rDA}	1,54E+11	s-1
E_{rDA}	9,42E+04	J/mol
R	8,3143	J mol-1 K-1

FGE-Jx+DPBM	$[F]_0$ / mol kg^{-1}	Error
FGE-J400	2,21	2.210 ± 0.016
FGE-J2000	1,089	1.089 ± 0.047
FGE-J4000	0,562	0.562 ± 0.060

Fig. S 3: Simulation for the DA-series: DPBM-FGE-J400, DPBM-FGE-J2000 and DPBM-FGE-J4000. (A) Equilibrium conversion x_{eq} as a function of temperature. **(B)** Evolution of the conversion $x(t)$ (blue) for a cooling from an equilibrium state at 80 °C to 25 °C with a cooling rate of -2 $K.min^{-1}$, as used in the SH-procedure. The equilibrium line (black) is given for reference.

Temperature profile of the self-healing procedure

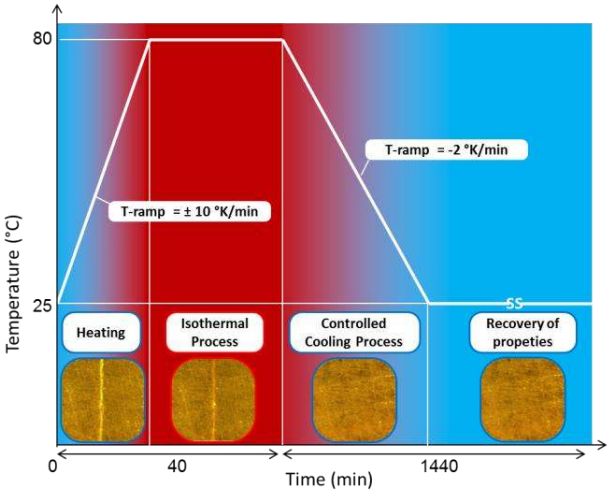

Fig. S 4: Temperature profile of the self-healing procedure, consisting of four phases: heating, isothermal phase, controlled cooling, and recovery of the mechanical properties.

The self-healing procedure used in practice to heal the damage to the actuators consists out of 4 phases (Fig. S 8): the heating phase (ca. 5 min), the isothermal phase (35 min), the controlled cooling phase (28 min), and the recovery phase for fully restoring the mechanical properties (ca. 24 h). This SH-procedure was used to heal the cuts made with the scalpel blade, as well as the perforations that occurred due to high overpressures. The images in Fig. S 8 are made using an optical microscope during the healing of a macroscopic cut (all the way through a 0.75 mm thick membrane, length = 14 mm and width = 0.17 mm) in a DPBM-FGE-J4000 sample. The images indicate that the cut could be completely healed.

Mechanical properties of the DA-material

Dynamic Mechanical Analysis (DMA):

The temperature-dependent visco-elastic properties of the Diels-Alder polymer series, including DPBM-FGE-J400, -J2000 and -J4000, were measured by DMA using a TA Instruments Q800 DMA for rectangular samples in tension mode (Fig. S 5). The measurement details are given in the caption. From the graphs in Fig. S 5, the glass transition temperature is taken as the temperature where the loss modulus reaches its maximum (solid blue line). The storage modulus, loss modulus and tan(δ) at 25 °C define the visco-elastic behaviour of the polymers at ambient temperature (dotted blue line). The characteristic parameters resulting from these measurements can be found in Table 1. The accelerating decrease of the moduli at temperatures above 70 °C is due to the gradually shifting equilibrium.

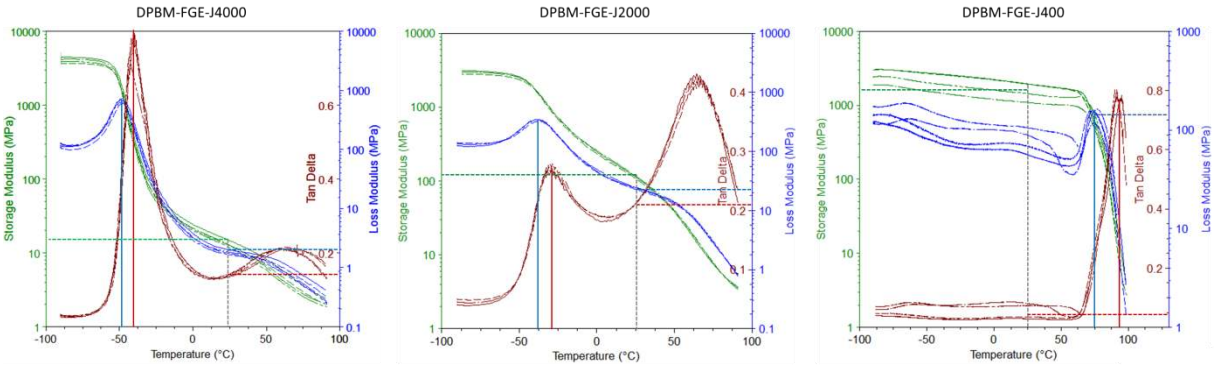

Fig. S 5: Temperature dependent visco-elastic behaviour for the DA-polymer series measured by DMA at an imposed oscillation strain 0.1 %, a frequency of 1 Hz, a static force 0.01 N and force tracking of 125%. Applied temperature profile: 1) equilibrate at -90 °C. 2) Isothermal at -90 °C for 5 min. 3) Ramp from -90 °C to 100 °C at 10 K.min^{-1}. Poisson ratio: 0.44 ± 0.01. Sample size in mm (thickness: t, width: w, length: l): 4 samples of DPBM-FGE-J4000 (t= 0.66; 0.68; 0.69; 0.70, w= 2.51; 2.79; 2.38; 3.20, l= 4.03; 3.99; 4.47; 4.45), 3 samples of DPBM-FGE-J2000 (t= 0.22; 0.22; 0.22, w= 3.11; 3.09; 2.90, l= 4.11; 3.90; 4.14) and 4 samples of DPBM-FGE-J400 (t= 0.39; 0.34; 0.56; 0.31, w= 2.09; 1.58; 2.66; 2.50, l= 3.60; 4.42; 4.58; 3.69).

Stress-strain curves:

The fracture strain and stress of the different polymers of the Diels-Alder series were measured on a TA Instruments Q800 DMA using a stress-strain test until fracture with rectangular samples in (Fig. S 6). The mean values and standard deviation of these measurements are presented in Table 1. It can be seen that the mechanical properties of the different DA-polymers differ a lot.

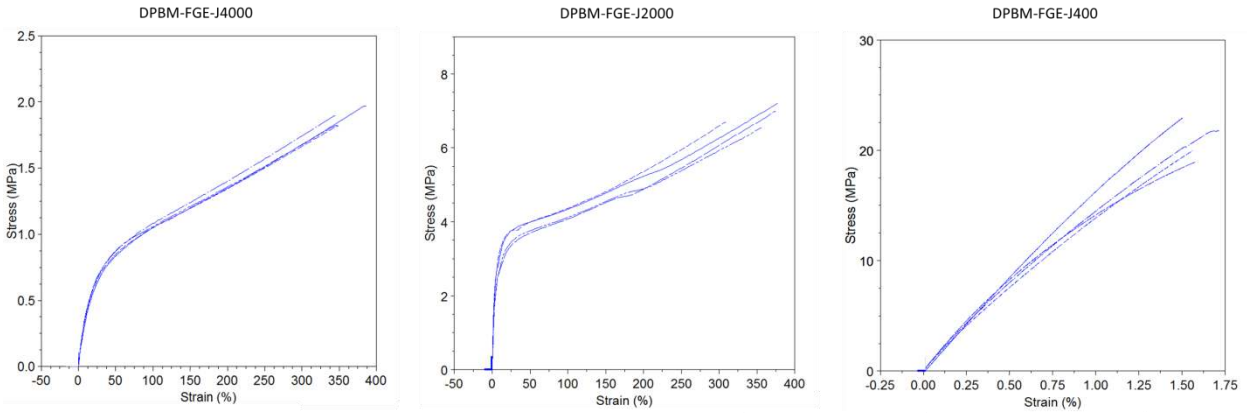

Fig. S 6: Stress strain curves for the DA-polymer series: imposed strain 0.1 %.min^{-1} (J400) or 65 %.min^{-1} (J2000 and J4000), 25 °C, Poisson ratio: 0.44 ± 0.01. Sample size in mm (thickness: t, width: w, length: l): 4 samples of DPBM-FGE-J4000 (t= 0.67; 0.67; 0.66; 0.66, w= 5.49; 4.49; 5.52; 5.54, l= 4.20; 4.20; 4.20; 4.18), 4 samples of DPBM-FGE-J2000 (t= 0.22; 0.22; 0.26; 0.32, w= 5.51; 5.51; 5.51; 5.51, l=4.19; 4.19; 4.02; 4.19) and 4 samples of DPBM-FGE-J400 (t= 0.25; 0.50; 0.24; 0.21, w= 2.26; 1.70; 1.86; 2.30, l= 4.17; 4.40; 4.37; 4.37).

Young's Modulus used in the simulation:

The FEM simulation in Abaqus used a static elastic model, taking only the elastic response of the flexible DA-polymer in account. The elastic deformation response is modelled using the Young's modulus of the DA-material,DPBM-FGE-J4000, which is obtained from a stress-strain curve (Fig. S 7) with a strain ramp of 65 %.min^{-1}, which roughly corresponds with the actuation speed of the prototypes. The DPBM-FGE-J2000 is strained with a ramp of 65 %.min^{-1} as well and the DPBM-FGE-J400 with a ramp of 0.1 %.min^{-1}. The Young's modulus is found through a linear regression over the strain interval (J4000: 0-5%, J2000: 0-2.5% and J400: 0-0.2%). A Young's modulus of 5.0 MPa is found for the DPBM-FGE-J4000, used in the soft actuators.

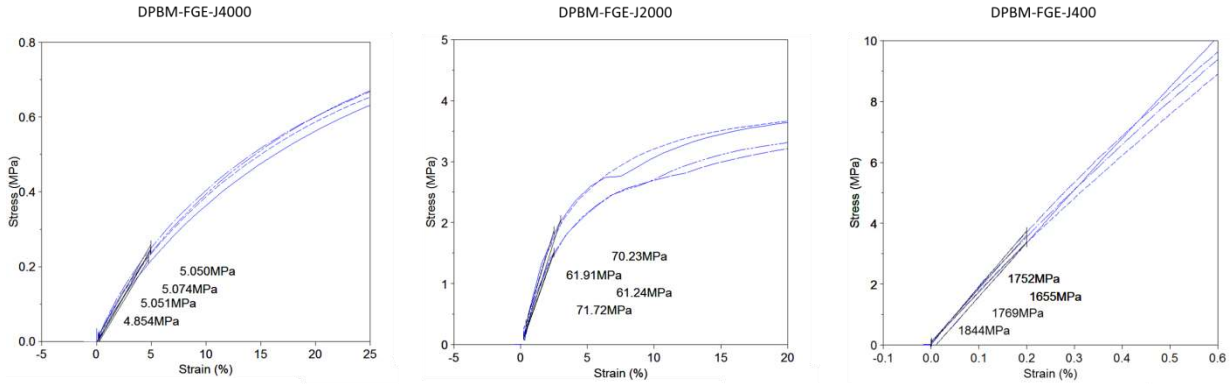

Fig. S 7: Young's Modulus determination of the DPBM-FGE-Jx, imposed strain 0.1 %.min^{-1} (J400) or 65 %.min^{-1} (J2000 and J4000), 25 °C, 0.44 ± 0.01. Sample size in mm (thickness: t, width: w, length: l): 4 samples of DPBM-FGE-J4000 (t= 0.67; 0.67; 0.66; 0.66, w= 5.49; 4.49; 5.52; 5.54, l= 4.20; 4.20; 4.20; 4.18), 4 samples of DPBM-FGE-J2000 (t= 0.22; 0.22; 0.26; 0.32, w= 5.51; 5.51; 5.51; 5.51, l=4.19; 4.19; 4.02; 4.19) and 4 samples of DPBM-FGE-J400 (t= 0.25; 0.50; 0.24; 0.21, w= 2.26; 1.70; 1.86; 2.30, l= 4.17; 4.40; 4.37; 4.37).

Gel temperature through dynamic rheometry:

The gel conversion (x_{gel}) and the corresponding equilibrium gel temperature (T_{gel}) are the conversion and temperature, respectively, at which an incipient network is formed in the reversibly crosslinking system (upon sufficiently slow cooling). At conversions above x_{gel}, the polymer will have a network structure and will behave as a solid. At conversions below x_{gel}, due to the too low crosslink density, the network has disintegrated into branched, linear, and/or small molecules, which results in a viscous behaviour. T_{gel} is important, since it defines the maximum temperature at which the DA-polymer still has a network structure and structural strength. If we heat the prototypes above this temperature, the polymer will start flowing and the structure will deform permanently and will eventually collapse. Therefor T_{gel} (Fig. S 8: DPBM-FGE-J4000 = 98 °C and DPBM-FGE-J2000 = 120 °C) it is recommended to always stay below this temperature during the self-healing procedure.

The gel temperature was measured by dynamic rheometry using a TA Instruments AR-G2 rheometer with a 14-mm disposable parallel plate setup (Fig. S 8). The equilibrium gel temperature T_{gel} was defined as the point where the loss angle (δ) is frequency independent in a multi-frequency experiment using 6 frequencies (19.85 Hz, 13.53 Hz, 9.22 Hz, 6.29 Hz, 4.28 Hz, 2.91 Hz, and 1.99 Hz), using an oscillating strain with an amplitude of 5 %, applied for temperatures from 80°C in steps of 2 K, waiting each time to reach equilibrium

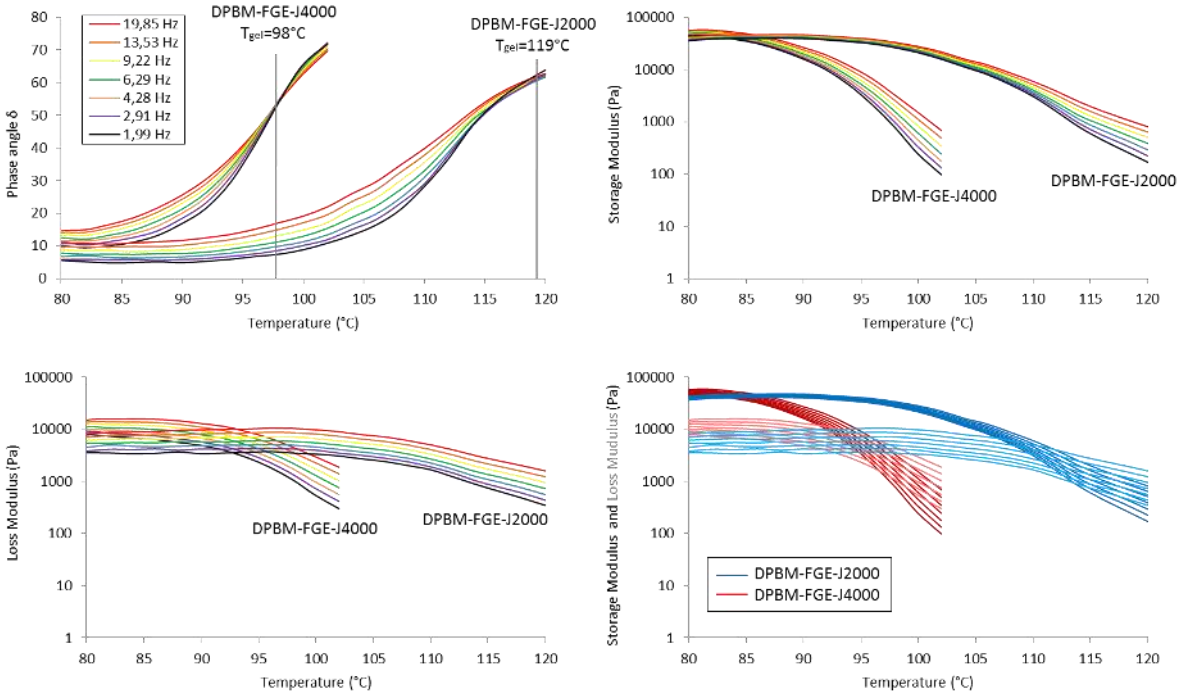

Fig. S 8: Measuring the gel temperature (T_{gel}) through dynamic rheometry of DPBM-FGE-J2000 (119°C) and DPBM-FGE-J4000 (98°C). The gel point is defined as the point where the loss angle (δ) is frequency independent. Measured for stepwise temperature increases of 2 K followed by a isothermal phase of 5 min from 80 °C to 102°C for the DPBM-FGE-J4000 and from 80°C to 120 °C in multifrequency measurement using 6 frequencies (19.85 Hz, 13.53 Hz, 9.22 Hz, 6.29 Hz, 4.28 Hz, 2.91 Hz, and 1.99 Hz), using an oscillating strain and an amplitude of 5%. Measured using disposable parallel with following sample dimensions in mm (d: diameter and t: thickness): DPBM-FGE-J4000 (d = 14 and t = 0.430) and DPBM-FGE-J2000 (d = 14 and t = 0.950).

FEM simulation in Abaqus

During the design phase of the prototypes, the large deformations of the bending soft pneumatic actuators (BSPAs) and the pleated pneumatic artificial muscles (PPAMs), resulting from pressurizing the membranes were modelled using a FEM model in an Abaqus environment. Only the elastic (time independent) response (represented by the storage modulus (E')) of the DPBM-FGE-J4000 DA-polymer was considered. In reality, the polymer has a visco-elastic response to an applied stress, however, the viscous part of the visco-elastic response (represented by the loss modulus (E")) was neglected in the simulation (at 25 °C the tan(δ)= *loss modulus(E")*/ *storage modulus(E')* = 0.14). The simulation is therefore quasi-static and purely elastic. Gravity is taken in account by accounting for the densities of the materials.

Geometries:

The 3D geometries were first designed in Autodesk Inventor and afterwards imported as step-files in Abaqus.

Material Parameters:

- DPBM-FGE-J4000: Young's Modulus = 5.0 MPa, Poisson ratio = 0.44 ± 0.01, Density: 1.05 g/ml
- Nylon cables: Young's Modulus = 100 MPa, Poisson ratio = 0.44, Density: 1.15 g/ml
- Flexible tube (Tygon R3603): Young's Modulus = 1.1 MPa, Poisson ratio = 0.44, Density: 1 g/ml

The density was measured by submerging weighed samples in water to measure their volume.

Solver

- Method: Direct, solution technique: Full Newton, DPB

The simulations were used during the design phase to tune the prototypes. The entire soft hand as well as the gripper were modelled. Two practical designs for the PPAM were found by modelling different muscles, which vary in membrane thickness, number of pleats, depth of the pleats and length.

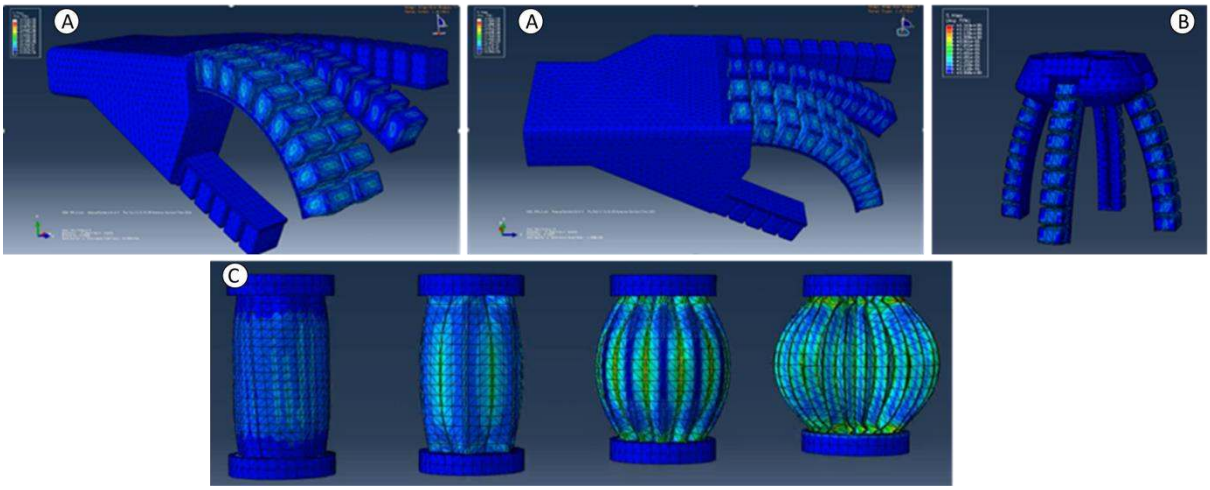

Fig. S 9: Simulating different designs for the self-healing soft robotic demonstrators using a static elastic model in Abaqus. (A) The soft pneumatic hand with fingers at overpressures of 25.0 kPa, 25.0 kPa, 11.0 kPa, and 0 kPa. **(B)** The soft gripper. **(C)** The pleated pneumatic artificial muscle 30.0 kPa.

Dimensions of the prototypes

Bending Soft Pneumatic Actuators (BSPA)

The parts in yellow on Fig. S 10 were constructed out of the most flexible DA-polymer, DPBM-FGE-J4000. The grey parts are non-self-healing flexible tubes made out of Tygon R3603. The dimensions indicated on Fig. S 10 are in mm.

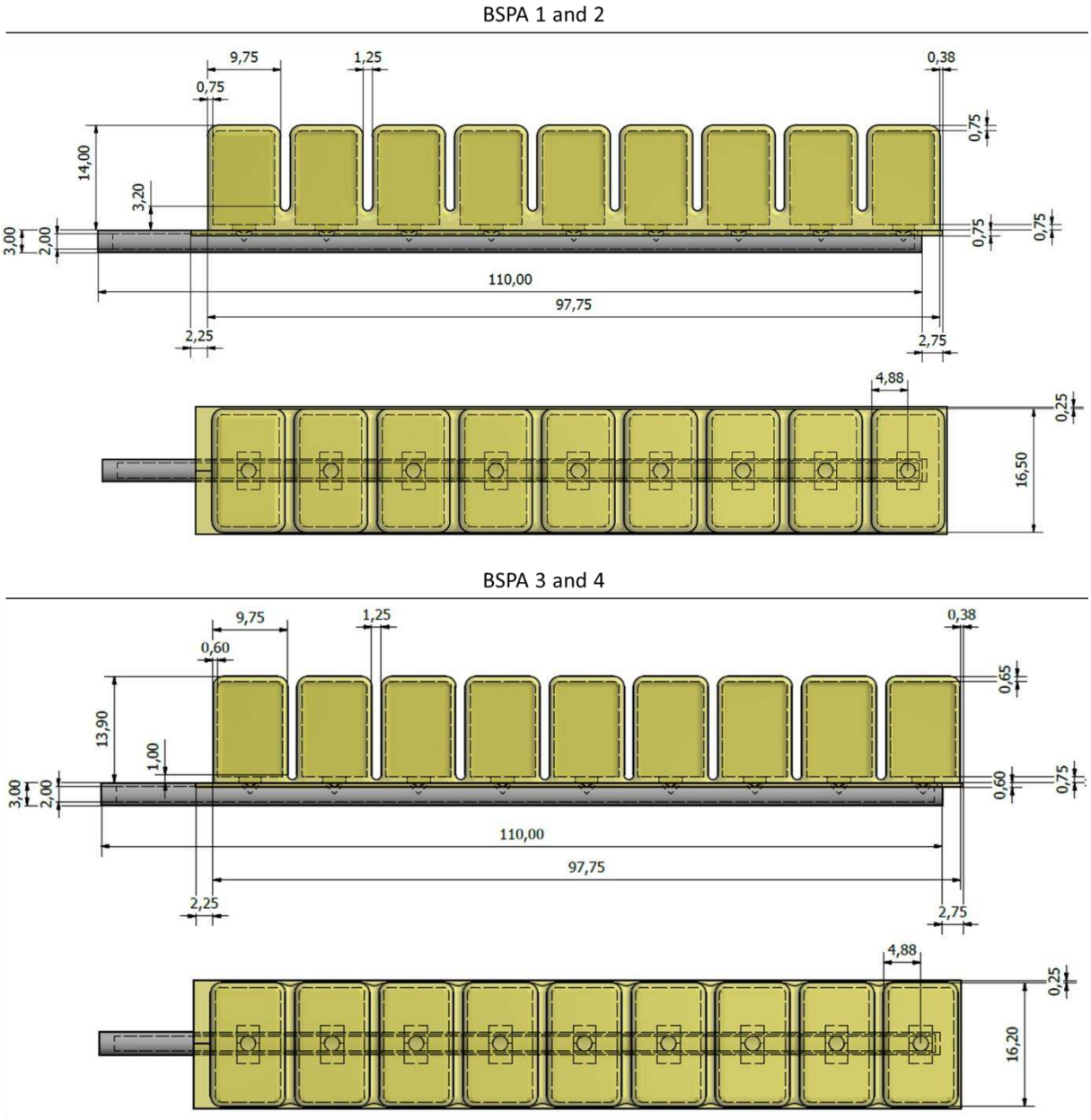

Fig. S 10: Dimensions of the two BSPA designs in mm.

Pleated Pneumatic Artificial Muscle (PPAM)

The parts in yellow on Fig. S 11 were constructed out of the most flexible DA-polymer, DPBM-FGE-J4000. The blue and green parts are non-self-healing 3D printed fittings (PLA material). The dimensions indicated on Fig. S 11 are in mm. Between the pleats of the pleated pneumatic artificial muscles, nylon cables are stretched along the creases to transmit the contraction force.

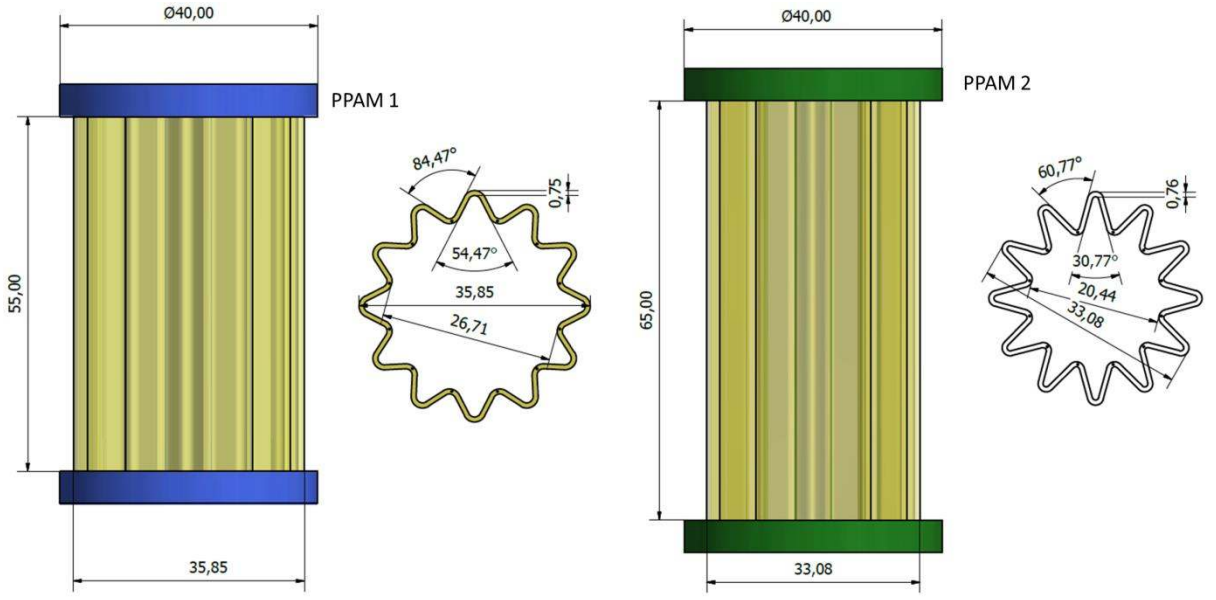

Specifications of the PPAMs			
		PPAM 1	PPAM 2
Sheet thickness	mm	0,75	0,75
Number of Pleats		12	12
Outer diameter (Do)	mm	36	33
Inner diameter (Di)	mm	27	20
Depth of the pleat (Do-Di)/2	mm	5	6
Length (without fittings)	mm	55	65

Fig. S 11: Dimensions of the two PPAM prototypes in mm.

Manufacturing of the SH-BSPA

Unlike soft (bodied) robots found in literature, which are mostly constructed from hyper elastic material through casting, the self-healing prototypes in this study were manufactured using the technique: "shaping-through-folding-and-self-healing" (Fig. S 12).

A. The flexible Diels-Alder polymers are synthesized in sheets through solvent-casting of the dissolved FGE-J4000 and DPBM from a 20 w% chloroform solution. A large surface is required to maximize the evaporation of chloroform from the network. The method of solvent-casting can therefore not be used for complex or thick 3D parts, since solvent will be trapped in the part leading to bubbles and cavities.
B. From the thin sheets (thickness: 0.60-0.75 mm) shapes can be cut using a scalpel blade, such as the plus-shaped geometry used for the cuboids.
C. The plus-shaped geometry can be folded into an open cuboid by placing it in a suitable Teflon mould.
D. The Teflon mould makes sure that the sides of the cuboid are pressed together such that these can be healed together using a first self-healing procedure (at 78°C for 2 hours, cooling at about 0.5 $Kmin^{-1}$).
E. After the self-healing procedure the sides of the cuboid are sealed and completely airtight.
F. The open cuboid is closed by a bottom DPBM-FGE-J4000 sheet. The connection is created and made airtight using a second healing procedure (110°C for a few seconds, using a soldering tool).
G. Using a scalpel blade a small opening is made in the bottom sheet to ensure the connection with the flexible tube (Tygon R3603) such that the cell (cuboid) can be pressurized.
H. 9 of these cells are made and placed in series.
I. To keep the cells in place, they will be placed in a Teflon holder.
J. The flexible tube (Tygon R3603) with openings cut-out to provide the connection between the 9 cells and the pressure source and is pressed in a hot DPBM-FGE-J4000 sheet to create the bottom layer of the BSPA.
K. The cells were placed on top of this bottom sheet by a third SH-procedure (78 °C for 30 min, cooling at about 0.5 $K.min^{-1}$) and everything was made airtight using a fourth SH-procedure (110°C for only seconds, using a soldering tool).

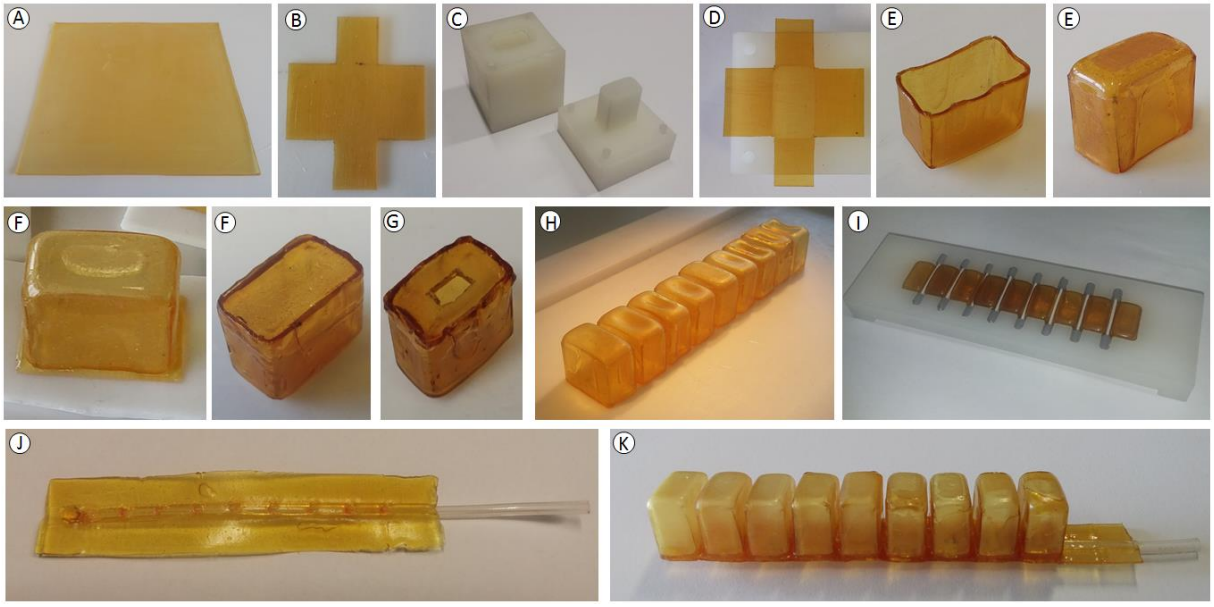

Fig. S 12: Constructing a BSPA using "shaping-through-folding-and-self-healing": (A) The DPBM-FGE-J4000 is synthesized in sheets. **(B)** A plus-shaped geometry can be cut out of the sheet. **(C and D)** This plus-shaped geometry can be folded inside of a Teflon mould. **(E)** After the first healing procedure (at 78°C for 2 hours, cooling at ± 0.5 $K.min^{-1}$) the sides of the open cuboid are sealed. **(F)** The cuboid is made completely airtight by a bottom sheet which is self-healed on the open cuboid with a second healing procedure (110°C for only seconds, using a soldering tool). **(G)** In order to pressurize the cells a hole was made at the bottom of the cell. **(H)** 9 cells were made and placed in series. **(I)** To keep the cells in place, they will be placed in a Teflon holder. **(J)** in a hot DPBM-FGE-J4000 a Tygon R3603 tube was pressed, which will provide the connection between the pressure source and the cells. **(K)** the cells were placed on top of this bottom sheet by a third SH-procedure (78 °C for 30 min, cooling at about 0.5 $K.min^{-1}$) and everything was made airtight using a fourth SH-procedure (110°C for only seconds, using a soldering tool).

Manufacturing of the SH-PPAMs

A. As for the BSPA, the manufacturing of the SH-PPAM starts with a flexible sheet of DPBM-FGE-J4000.
B. This sheet was placed around a 3D printed (black) cylindrical part that has a star-shaped cross section. The sheet is pulled against this part by tightening nylon cables along the creases. The star-shaped tube of the DA-polymer is closed by self-healing the two ends together, using a local heating procedure (at 110 °C for a few seconds). Subsequently the part was exposed to a second SH-procedure by placing it in an oven at 80 °C.
C. Because of the relaxation of the forces during this healing process, the creases are formed permanently in the sheet
D. Next, nylon wires were stretched along the creases to generate the contraction force when the muscle is pressurized.
E. On both sides, 3D printed fittings are placed and the muscle is made airtight using a last SH-procedure.
F. The cables are fixed inside the fitting by epoxy-amine glue.
G. The pleated pneumatic artificial muscle (PPAM 1) is completed by placing a tube in the fittings that connects the muscle to a pressure source.
H. Image of PPAM 2, having slightly different dimensions.

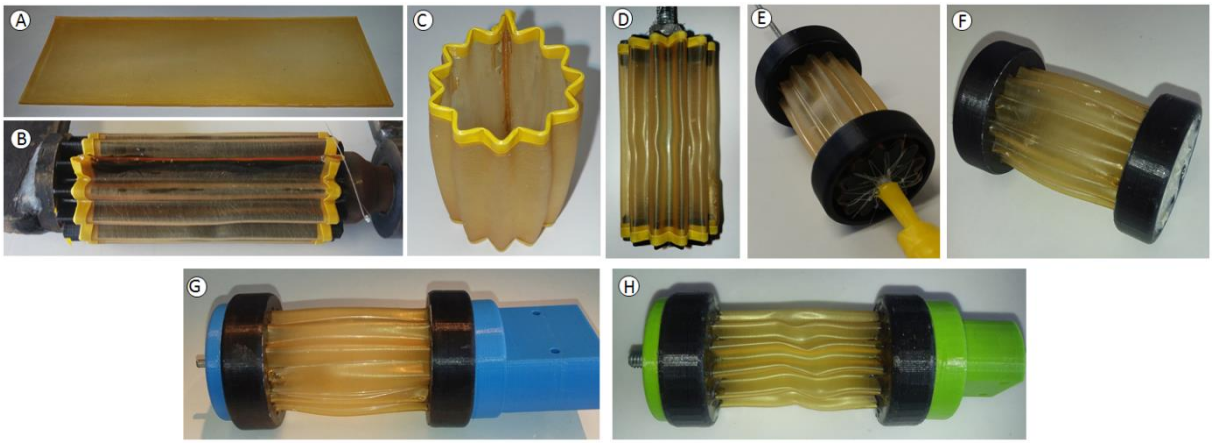

Fig. S 13: "Shaping-through-folding-and-self-healing" to manufacture the PPAMs. (A) The DPBM-FGE-J4000 is synthesized through solvent casting in sheets. **(B)** Creases are folded in the sheet and the cylindrical shape is closed by self-healing the two ends together using a local SH-procedure. Next, the piece is exposed to a global SH-procedure by heating in an oven. **(C)** After this, the creases are formed permanently. **(D)** Nylon wires are stretched along the creases. **(E and F)** Fittings are placed on both sides to make the muscle airtight. **(G and H)** Two SH-prototypes; PPAM 1 and PPAM 2.

Dedicated test bench

The overpressure can be regulated by the simultaneous work of an inlet, connected to a pressure source, and an outlet solenoid valve, connected to atmospheric pressure. These valves are switching at high frequency using PWM controlled Power FET Switches. The pressure inside is adjusted by the duty cycles of the PWM signals of the inlet and outlet valve. The deformations were captured using a digital camera, while the forces exerted by the tip of the actuator were measured using a load cell (Futek LSB200, 2 lb). To control the actuator movement in the soft hand and the soft gripper, a setup was built in which 5 overpressures can be regulated individually using 5 control systems. Each system contains 2 solenoid valves, 2 Power FET switches, 2 PWMs and a buffer volume.

Pressure controller:

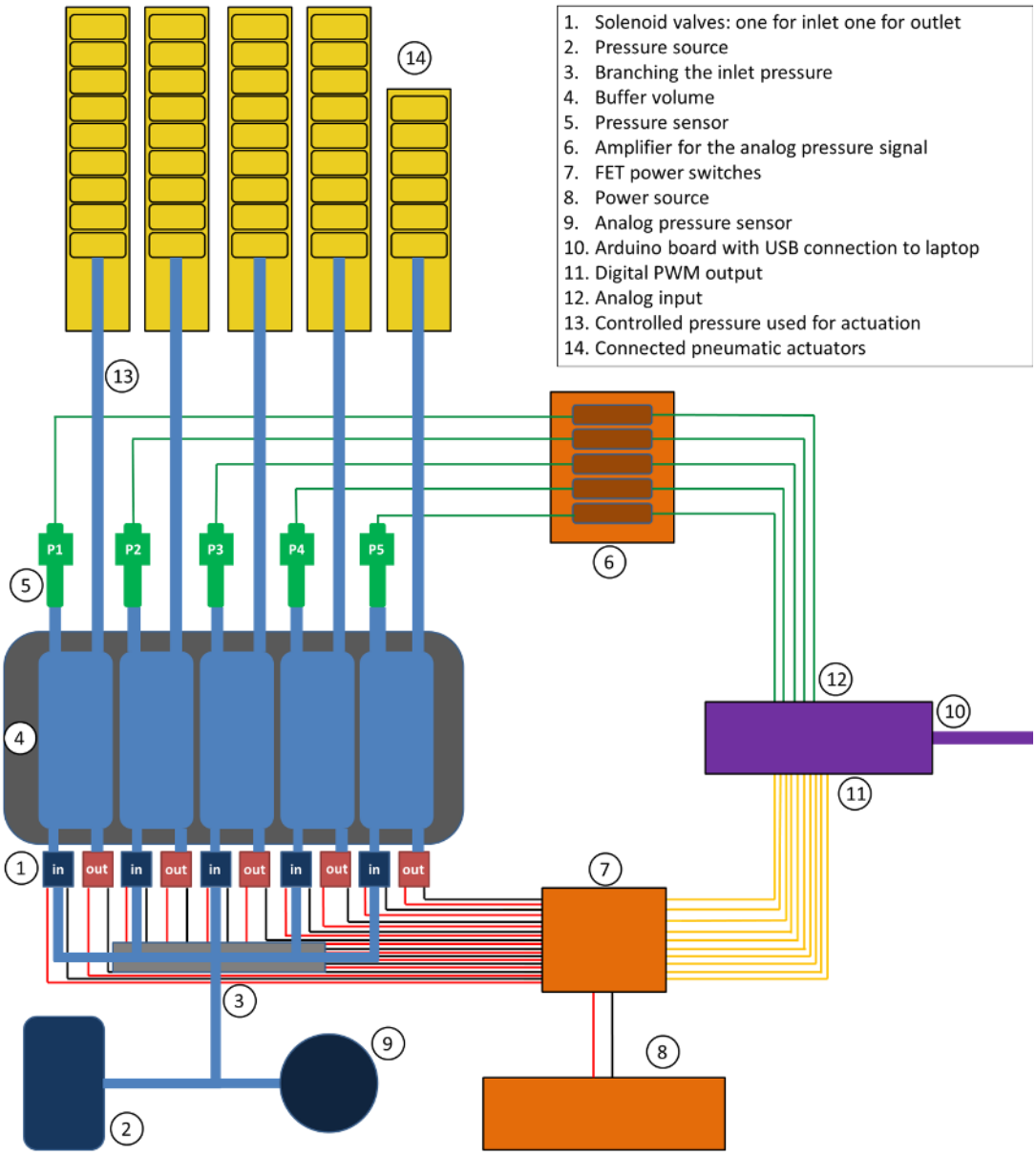

Fig. S 14: Pressure control system scheme.

Components:

- Power FET Switches: MOSFET 4 v04
- Arduino Mega ADK
- Honeywell Differential Pressure Sensor (maximum reading: 15psi, 10 V dc)
- Analog Devices AD623ANZ, Instrumentation Amplifier
- Solenoid Valve: Matrix 720 Series compact (0-6 bar)
- Power Source: 12V

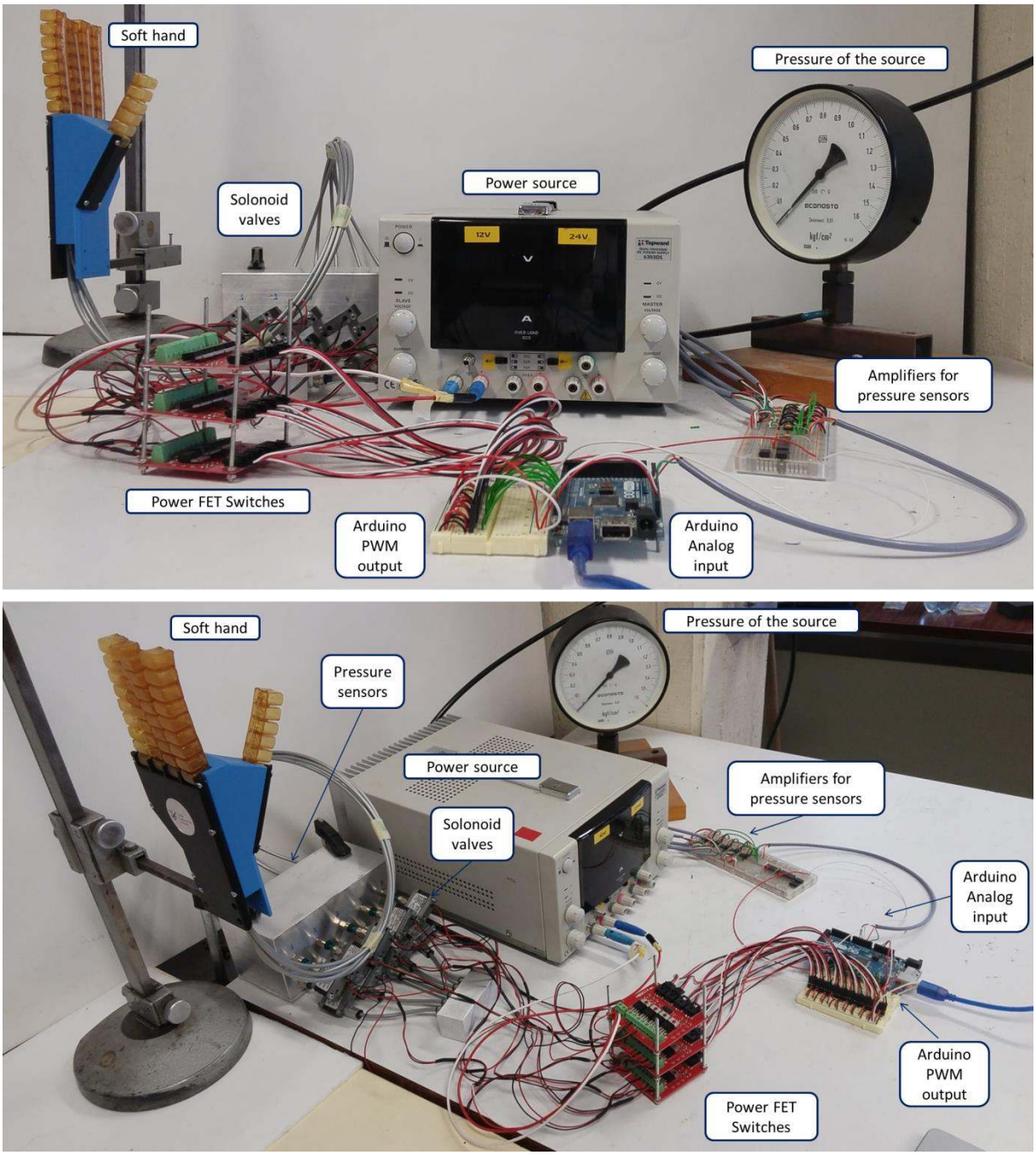

Fig. S 15: Images of the pressure control system.

Images:

- Images for measuring the deformations were taken using a digital camera.

Forces:

- Using two different load cells;
  - FUTEK LSB200 , 2 lb
  - FUTEK LSB200 , 50 lb
- The load cell signals were amplified using FUTEK Amplifier Module CSG110.

Measuring the efficiency of the self-healing procedure

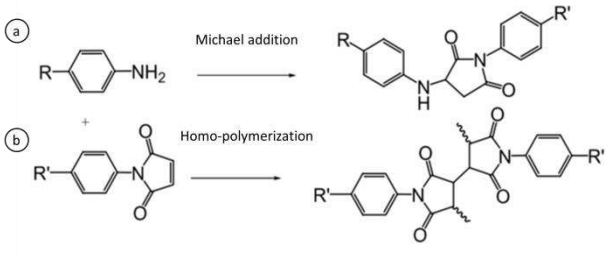

Fig. S 16: Irreversible crosslinking of bismaleimide networks via a combination of Michael addition and maleimide homo-polymerization.

In this study, we show that keeping the DA-polymers at high temperature (above 80 °C) for more than 1 hour leads to a small loss in SH-ability and a small change in mechanical properties of the Diels-Alder polymer, and more specifically for the DPBM-FGE-J4000. The glass transition temperature remains approximately the same, but both the storage modulus and loss modulus decrease when the material is exposed for to high temperature. It is believed that 2 different reaction mechanisms contribute to the forming of irreversible bonds: Michael addition of remaining amine and maleimide and the homo-polymerization of maleimide leads to a reduced cross-link density (Fig. S 16).

The Michael addition takes place between an amine and a maleimide. Amine can be present in the system if some of the Jeffamine's amino groups did not react with furfuryl glycidyl ether (FGE) in the first (irreversible) reaction step of the synthesis, due to a shortage of FGE. Therefor it can be useful to use a little excess of FGE in this reaction step (not done in the synthesis in this study). Amine can also be present in the maleimide as an impurity. It is therefore important that the reactions are done with bismaleimide with a high purity. The Michael addition takes place at relative low temperatures (already at 80 °C). The homopolymerization of maleimide occurs at higher temperatures (T > 100 °C) in the absence of initiators and catalysts (not used in this research).

Both reactions, the homopolymerization and the Michael addition, decrease the number of reversible cross-links in the polymer network: the homopolymerization by consuming maleimide groups and creating an imbalance in the furan/maleimide group molar ratio, while the Michael addition creates irreversible cross-links if Jeffamine amino groups are involved. Due to a decrease in cross-link density, the elastic modulus in the rubber state decreases.

Because mechanical properties drop slightly as a function of SH-cycles, we introduced the recovery-efficiency based on the storage modulus (*E*') and defined as:

$$\eta_{SH} = \left(1 - \frac{E'_{before\ SH} - E'_{after\ SH}}{E'_{before\ SH}}\right) * 100$$

This recovery-efficiency (η_{SH}) is 93.4% in average over the various damage-healing-cycles. The homopolymerization and Michael addition take place during the isothermal stage at 80 °C in the SH-procedure. The duration of the isothermal process in the damage-healing-cycles, 4 hours during the SH-testing, is rather long compared to healing in practice, in which this stage is usually limited to 40 min. Therefore, for healing in practice the SH-efficiency will be above 93.4 %, typically closer to 98-99%, as long as the temperature is limited to 80 °C.

Recycling of the Diels-Alder Polymers

An additional advantage of the Diels-Alder network is that due to their reversible nature, they can be dissolved and recycled. To prove this, cells intended for the manufacturing of a BSPA and made out of DPBM-FGE-J4000 were cut into small pieces (Fig. S 17). These were swelled and dissolved in chloroform (20 w%). To decrease the duration of this process, the mixture was brought at 65 °C (for 24 h). When completely dissolved, the solution could be solvent-cast into a sheet again. With this sheet new cells could be manufactured, which were used in the 6 cell BSPA prototype; the thumb of the soft hand.

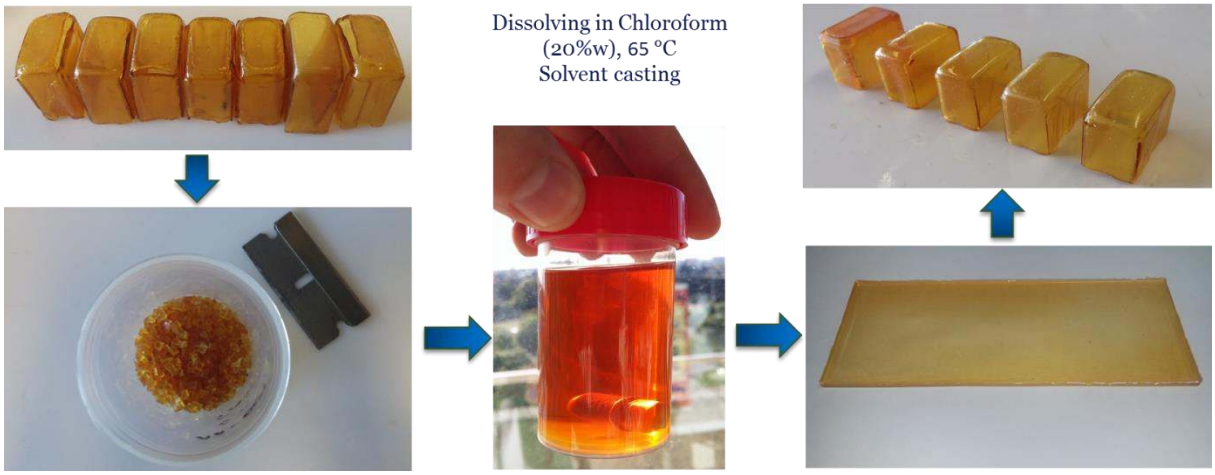

Fig. S 17: Diels-Alder polymer waste of the manufacturing process of the prototypes can be recycled. This was proven by recycling the DPBM-FGE-J4000 cuboid cells. The cells were cut into small pieces and these were subsequently swelled and dissolved in chloroform (20 w%). To increase accelerate the dissolving, the mixture was heated up to 65 °C. A sheet (0.75 mm) was solvent-cast and from this sheet cells were constructed.

It was important to check whether the mechanical properties were recovered after the recycling procedure. Therefore, the visco-elastic and mechanical properties of the recycled sheet were measured using DMA and compared with the properties of the two original batches (Fig. S 18). The glass transition temperature (T_g) is about 5 K lower and the storage modulus decreased by about 81 %. As for the SH-procedure, increasing the temperature during the dissolution process leads to faster kinetics of the Michael addition reaction and the homopolymarization. When these reactions occur, the reversible DA-crosslinks are exchanged for irreversible crosslinks or chain extension reactions, which leads to overall to a drop in storage modulus and a reduction of the self-healing ability. This change in properties can be minimized by decreasing the temperature during dissolving to room temperature, though in that case, the swelling and dissolving of the polymer parts will take longer. If bismaleimide is used with a higher purity, the side reactions will be minimized as well. Nonetheless, even in these non-optimal conditions, it is proven that the SH-soft robotic parts can be recycled.

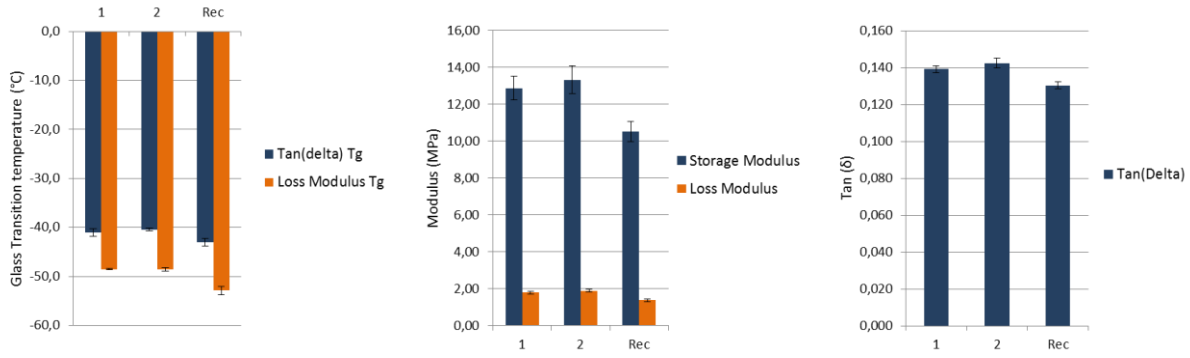

Fig. S 18: Recovery of the material properties after the recycling procedure. The Glass transition temperature and visco-elastic properties at 25 °C for the recycled DPBM-FGE-J4000 sheet (Rec) are compared with the two original batches (1 and 2). For each material, 4 samples were measured of which the mean and standard deviation are presented in the graphs.